3-15-1999

Semianalytic Moderate-Resolution Imaging Spectrometer Algorithms for Chlorophyll *a* and Absorption with Bio-Optical Domains Based on Nitrate-Depletion Temperatures

Kendall L. Carder
University of South Florida, kcarder@marine.usf.edu

F. R. Chen
University of South Florida

Z. P. Lee
University of South Florida

S. K. Hawes
University of South Florida

D. Kamykowski
North Carolina State University

JOURNAL OF GEOPHYSICAL RESEARCH, VOL. 104, NO. C3, PAGES 5403–5421, MARCH 15, 1999

Semianalytic Moderate-Resolution Imaging Spectrometer algorithms for chlorophyll *a* and absorption with bio-optical domains based on nitrate-depletion temperatures

K. L. Carder, F. R. Chen, Z. P. Lee, and S. K. Hawes

Department of Marine Science, University of South Florida, St. Petersburg

D. Kamykowski

Department of Marine, Earth, and Atmospheric Sciences, North Carolina State University, Raleigh

Abstract. This paper describes algorithms for retrieval of chlorophyll *a* concentration and phytoplankton and gelbstoff absorption coefficients for the Moderate-Resolution Imaging Spectrometer (MODIS) or sensors with similar spectral channels. The algorithms are based on a semianalytical, bio-optical model of remote sensing reflectance, $R_{rs}(\lambda)$. The $R_{rs}(\lambda)$ model has two free variables, the absorption coefficient due to phytoplankton at 675 nm, $a_\phi(675)$, and the absorption coefficient due to gelbstoff at 400 nm, $a_g(400)$. The R_{rs} model has several parameters that are fixed or can be specified based on the region and season of the MODIS scene. These control the spectral shapes of the optical constituents of the model. $R_{rs}(\lambda_i)$ values from the MODIS data processing system are placed into the model, the model is inverted, and $a_\phi(675)$, $a_g(400)$, and chlorophyll *a* are computed. The algorithm also derives the total absorption coefficients $a(\lambda_i)$ and the phytoplankton absorption coefficients $a_\phi(\lambda_i)$ at the visible MODIS wavelengths. MODIS algorithms are parameterized for three different bio-optical domains: (1) high photoprotective pigment to chlorophyll ratio and low self-shading, which for brevity, we designate as "unpackaged"; (2) low photoprotective pigment to chlorophyll ratio and high self-shading, which we designate as "packaged"; and (3) a transitional or global-average type. These domains can be identified from space by comparing sea-surface temperature to nitrogen-depletion temperatures for each domain. Algorithm errors of more than 45% are reduced to errors of less than 30% with this approach, with the greatest effect occurring at the eastern and polar boundaries of the basins.

1. Introduction

According to the optical classification by *Morel and Prieur* [1977], oceanic waters may be characterized as case 1, in which the optical properties are dominated by chlorophyll and associated and covarying detrital pigments, or as case 2, in which other substances, which do not covary with chlorophyll, also affect the optical properties. Such substances include gelbstoff, suspended sediments, coccolithophores, detritus, and bacteria. Pigment retrievals from Coastal Zone Color Scanner (CZCS) data in case 1 waters have achieved reasonable results (± 40% for local best cases [*Gordon et al.*, 1983]). However, substances not covarying with chlorophyll in case 2 waters have caused the retrieval of pigment concentrations to have inaccuracies as high as 133% [*Carder et al.*, 1991].

Marine colored dissolved organic matter (CDOM), also called gelbstoff, absorbs light in an exponentially decreasing manner as a function of wavelength. Pheopigments, detritus, and bacteria similarly absorb more strongly at 412 nm than they do at 443 nm. Phytoplankton, on the other hand, absorb more strongly at 443 nm than at 412 nm. Thus, by measuring the relative amounts of light leaving the sea surface at those two wavelengths, we can estimate the relative amounts of phytoplankton and the other absorbing products mentioned above.

CDOM has classically been thought of as a terrigenous product, but it is also produced when grazing, photolysis, and other mechanisms degrade the viable plant matter at and downstream from phytoplankton blooms. The CDOM-to-chlorophyll ratio for coastal regions can change dramatically for a parcel of upwelled water over a relatively short time, from chlorophyll rich and CDOM poor to CDOM rich and chlorophyll poor. Solid evidence for the occurrence of this scenario can be found in two separate studies. *Peacock et al.* [1988] found that absorption attributed to CDOM at 440 nm was at least sixteenfold that due to phytoplankton pigments within an offshore jet from an upwelling region, whereas pigments were the dominant absorption agents at the upwelling center near the coast. Similarly, *Carder et al.* [1989] found that particulate absorption at 440 nm decreased thirteenfold while CDOM absorption at 440 nm increased by 60% in 10 days for a phytoplankton bloom tracked from the Mississippi River plume to Cape San Blas. This widely varying CDOM-to-chlorophyll ratio has a profound effect on upwelled radiance in the blue 443 nm band of the CZCS and a smaller but still significant

Paper number 1998JC900082.
0148-0227/99/1998JC900082$09.00

effect at the 488 and 531 nm bands of MODIS. The correspondence in absorption at 443 and 488 nm between CDOM and chlorophyll creates erroneously high estimates of pigment concentration in those models that rely solely upon either of these spectral bands to indicate absorption due to phytoplankton.

Winter convective over turn of the upper ocean layer also mixes up gelbstoff-rich deeper waters that have not been photo bleached as have summer surface waters. These waters appear in CZCS data as being more chlorophyll rich than measurements and models indicate [*Siegel and Michaels*, 1996].

The remote sensing reflectance R_{rs} model used to develop the algorithm presented here has a few parameters that cannot be fixed and applied to the entire globe; that is, they are site and season specific. This is due to the inherent variability of many bio-optical constituents. For example, absorption at 440 nm per unit chlorophyll *a* by phytoplankton can change with species and with nutrient and lighting conditions by as much as a factor of 5 [*Morel and Bricaud*, 1981; *Kirk*, 1983; *Carder et al.*, 1991; *Morel et al.*, 1993]. In addition, particle size and concentration have significant effects on the spectral backscattering coefficient $b_b(\lambda)$ of ocean water; pure water backscatter varies as ~ λ^{-4}, large-particle backscatter varies as ~ λ^{0}, and backscatter by smaller-diameter detritus and bacteria varies with a spectral dependence between the two extremes [*Morel and Ahn*, 1990, 1991].

Many of these factors covary, allowing the simple wavelength-ratio algorithms of the CZCS [*Gordon and Morel*, 1983] to work fairly well. We have tried to understand many of these individual covariances and have developed empirical expressions for several individual bio-optical variables. By analyzing individual components of the model, we can gain a deeper understanding of the processes affecting the color of water-leaving radiance.

To the extent that such covariances change with season or bio-optical domains [e.g., see *Prieur and Sathyendranath*, 1981; *Sathyendranath et al.*, 1989; *Mitchell and Holm-Hansen*, 1991], we must consider temporal and spatial changes in algorithm parameterization. A strategy for partitioning the ocean into at least three different bio-optical domains on the basis of nutrient-temperature relationships, each with different model parameters, is discussed in section 5. Initially, model development is focused on tropical and subtropical environments.

The main data product of the algorithm is chlorophyll *a* concentration [chl *a*], which can be used as an indicator of plankton biomass, as an input to primary production models, or to trace oceanographic currents, jets, and plumes. Other output products are the absorption coefficients $a_\phi(675)$, $a_g(400)$, $a_\phi(\lambda_i)$, and $a(\lambda_i)$. Here $a_\phi(\lambda_i)$ is used in the Moderate-Resolution Imaging Spectrometer (MODIS) algorithm for fluorescence efficiency; $a_g(400)$ by itself can be used to map river plumes, to determine diffuse attenuation at that wavelength, or to calculate dissolved organic carbon (DOC) standing stocks and fluxes [*Carder et al.*, 1991]. In order to calculate DOC, we need to know how DOC concentration is related to DOC absorption. As coastal, estuarine, and other case 2 environments become increasingly recognized as important areas of study, algorithms that can deal with the complex bio-optical properties of these regions are required.

2. Instrument Characteristics

The algorithm requires input of the water-leaving radiance L_w at the MODIS ocean wave bands centered at 412, 443, 488, and 551 nm, respectively, and bio-optical domains are designated based upon sea-surface temperature (section 5), a derived product of MODIS. R_{rs} is derived from the water-leaving radiance L_w [*Gordon and Wang*, 1994], as $R_{rs} = L_w(F_0 \cos\theta)^{-1}$, where F_0 is the extraterrestrial solar irradiance and θ is the solar zenith angle. The 1000 m resolution, new spectral bands, and near-daily coverage of MODIS will allow the observation of mesoscale oceanographic features in coastal and estuarine environments, areas seen to be increasingly important in many marine science studies in addition to traditional open-ocean observations.

3. Algorithm Description

3.1. Theoretical Basis

Morel and Gordon [1980] describe three approaches to interpret ocean color data in terms of the in situ optical constituents: empirical, semiempirical, and analytical. In the analytical approach, radiative transfer theory provides a relationship between upwelling irradiance or radiance and the in situ constituents [e.g., *Sathyendranath and Platt*, 1997]. Then, constituent concentrations are derived from irradiance or radiance values measured at several wavelengths by inversion of the resultant system of equations. The MODIS algorithm uses this approach, with the term "semi analytical" invoked because bio-optial pieces of the radiative model are expressed by empirical relationships.

After light enters the ocean, some of it is eventually scatters back up through the surface. This light is called the water-leaving radiance $L_w(\lambda)$, and it can be deduced from space after removal of atmospheric effects. The magnitude, spectral variation, and angular distribution of this radiance depend on the following factors: the absorption and backscattering coefficients of the seawater, $a(\lambda)$ and $b_b(\lambda)$, respectively (known as the inherent optical properties); the downwelling irradiance incident on the sea surface $E_d(\lambda,0^+)$; and the angular distribution of the light within the ocean. To make things easier, we divide seawater into three components, each one having distinct optical properties of its own. These components are the seawater itself (water and salts), the particle fraction, and the dissolved fraction. Fortunately, $a(\lambda)$ is simply equal to the sum of the absorption coefficients for each component, and $b_b(\lambda)$ is equal to the sum of the backscattering coefficients. If we can accurately describe or model each spectrally distinct component of the absorption and backscattering coefficients, then we can determine the magnitude of each one from measurements of $L_w(\lambda)$ and $E_d(0^+,\lambda)$, given some assumptions about the angular distribution of light in the water. The key here is to accurately model the spectral behavior of $a(\lambda)$ for each component. The spectral behavior of $b_b(\lambda)$ is not as dynamic.

The R_{rs} model is given by the following general equation, which is adapted from *Lee et al.* [1994]:

$$R_{rs}(\lambda) = \frac{f\,t^2}{Q(\lambda)\,n^2}\frac{b_b(\lambda)}{[a(\lambda) + b_b(\lambda)]} \qquad (1)$$

where f is an empirical factor averaging about 0.32–0.33 [*Gordon et al.*, 1975; *Morel and Prieur*, 1977; *Jerome et al.*, 1988; *Kirk*, 1991], t is the transmittance of the air-sea interface, $Q(\lambda)$ is the upwelling irradiance-to-radiance ratio $E_u(\lambda)/L_u(\lambda)$, and n is the real part of the index of refraction of seawater. By making three approximations, (1) can be greatly simplified.

1. In general, f is a function of the solar zenith angle θ_0 [*Kirk*, 1984; *Jerome et al.*, 1988; *Morel and Gentili*, 1991]. However, *Morel and Gentili* [1993] have shown that the ratio f/Q is relatively independent of θ_0 for Sun and satellite viewing angles expected for the MODIS orbit. They estimate that f/Q = 0.0936, 0.0944, 0.0929, and 0.0881 (standard deviation ± 0.005), for λ = 440, 500, 565, and 665 nm, respectively. Also, *Gordon et al.* [1988] estimates that f/Q = 0.0949 for $\theta_0 \geq 20°$. Thus we assume that

f/Q is independent of λ and θ_0 for all MODIS wave bands of interest, except perhaps for the band centered at 667 nm. The spectral behavior of f/Q near this wavelength is not a problem since this band is not used in the algorithms because of the strong absorption there by water molecules.

2. Here t^2/n^2 is approximately equal to 0.54, and although it can change with sea state [*Austin*, 1974], it is relatively independent of wavelength.

3. Many studies have confirmed that $b_b(\lambda)$ is usually much smaller than $a(\lambda)$ and can thus be safely removed from the denominator of (1) [*Morel and Prieur*, 1977; *Gordon and Morel*, 1983, and references therein), except for highly turbid waters.

These three approximations lead to a simplified version of (1),

$$R_{rs}(\lambda) \approx cons \frac{b_b(\lambda)}{a(\lambda)} \quad (2)$$

where the "constant" is unchanging with respect to λ and θ_0. The value of the constant is not relevant to the algorithm since, as will be shown later, the algorithm uses spectral ratios of $R_{rs}(\lambda)$ and the constant term factors out.

3.2. Backscattering Term

The total backscattering coefficient $b_b(\lambda)$ can be expanded as

$$b_b(\lambda) = b_{bw}(\lambda) + b_{bp}(\lambda) \quad (3)$$

where the subscripts w and p refer to water and particles, respectively. The $b_{bw}(\lambda)$ is constant and well known [*Smith and Baker*, 1981]; $b_{bp}(\lambda)$ is modeled as

The magnitude of particle backscattering is indicated by X, which is equal to $b_{bp}(551)$, while Y describes the spectral shape of the particle backscattering.

$$b_{bp}(\lambda) = X \left[\frac{551}{\lambda}\right]^Y \quad (4)$$

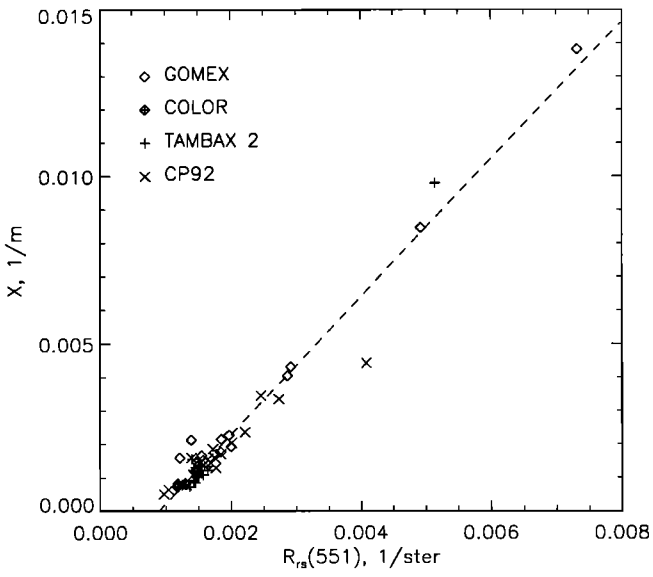

Figure 1. X versus $R_{rs}(551)$, where X is the magnitude of particle backscattering and R_{rs} is the remote sensing reflectance at 551 nm wavelength. The line is the linear regression equation $X = -0.00182 + 2.058\ R_{rs}(551)$ (number of samples $n = 53$, correlation coefficient $r^2 = 0.96$).

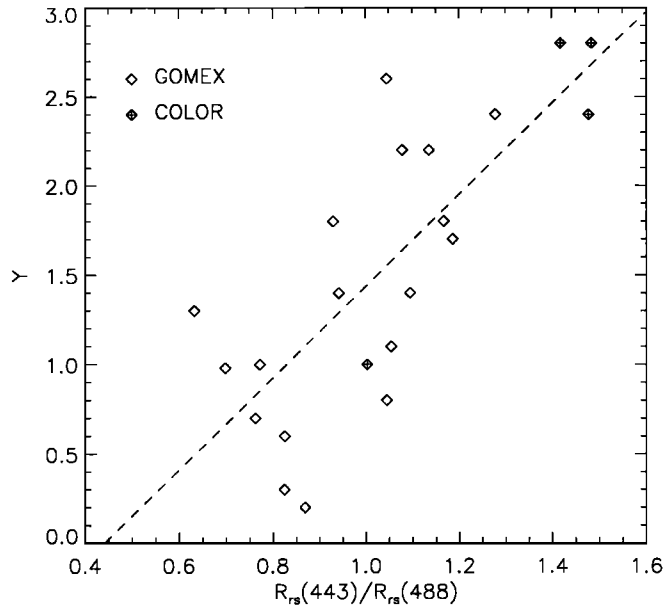

Figure 2. Spectral shape of particle backscattering Y versus $R_{rs}(443)/R_{rs}(488)$. The line is the linear regression $Y = -1.13 + 2.57\ R_{rs}(443)/R_{rs}(488)$ ($n = 22$, $r^2 = 0.59$).

Lee et al. [1994] empirically determined X and Y values by model inversion using a formula similar to (4). The X and Y values were compared to the $R_{rs}(\lambda)$ values measured at each station with the purpose of finding empirical relationships for both X and Y as a function of $R_{rs}(\lambda)$ at one or more of the MODIS wavelengths. Once this was done, X and Y could be estimated from MODIS data. These empirical relationships are described below.

The general expression for X is

$$X = X_0 + X_1 R_{rs}(551) \quad (5)$$

where X_0 and X_1 are empirically derived constants. Linear regression performed on the derived values of X versus $R_{rs}(551)$ taken from four cruises to the Gulf of Mexico (CP92, Tambax 2, GOMEX, and COLOR) resulted in X_0 and X_1 values of -0.00182 m^{-1} and 2.058 sr m^{-1} (number of samples $n = 53$, correlation coefficient $r^2 = 0.96$). Figure 1 shows the regression graphically. If X is determined to be negative from (5), it is set to zero.

Y was found to covary in a rather general way with the ratio $R_{rs}(443)/R_{rs}(488)$. Variations in numerator and denominator values of this ratio are largely determined by absorption due to phytoplankton and CDOM. Absorption due to water is about the same and low at both wavelengths. Thus, to the extent that phytoplankton and CDOM absorption covary, the spectral ratio of the absorption coefficients, $a(443)/a(488)$, will be only weakly dependent on pigment concentration, and the spectral ratio of backscattering coefficients should have a significant effect on the spectral ratio of R_{rs}. Y is thus represented as a linear function of $R_{rs}(443)/R_{rs}(488)$,

$$Y = Y_0 + Y_1 \frac{R_{rs}(443)}{R_{rs}(488)} \quad (6)$$

where Y_0 and Y_1 are empirically derived constants.

Accurate measurements of $a_g(\lambda)$ and accurate removal of reflected skylight from the R_{rs} measurements are critical in determining Y by model inversion. Only data from the GOMEX and COLOR cruises are used here because the $a_g(\lambda)$ values were

determined with a long-path spectrophotometer [*Peacock et al.*, 1994]. Linear regression of Y versus $R_{rs}(443)/R_{rs}(488)$ for stations from these two cruises resulted in Y_0 and Y_1 values of -1.13 m^{-1} and 2.57 m^{-1} ($n = 22$, $r^2 = 0.59$). Figure 2 shows the regression graphically. If Y is determined to be negative from (6), it is set to zero. A number of other spectral ratios of $R_{rs}(\lambda)$ were tested, but the 443:488 ratio had the highest correlation with Y.

The Y parameter should be large when the backscattering is due to small particles and/or water and vice versa [*Gordon and Morel*, 1983]. In oligotrophic regions we have determined values of Y greater than 2, while in waters with [chl *a*] > 10 mg m^{-3} the estimated Y values are often ≈ 0. Where gelbstoff concentrations are high, pigments are more packaged, so larger particles and lower Y values are expected to occur here, even with a lack of covariation between pigment and gelbstoff absorption.

3.3. Absorption Term

The total absorption coefficient can be expanded as

$$a(\lambda) = a_w(\lambda) + a_\varphi(\lambda) + a_d(\lambda) + a_g(\lambda) \quad (7)$$

where the subscripts w, ϕ, d, and g refer to water, phytoplankton, detritus, and gelbstoff (CDOM). Here $a_w(\lambda)$ is taken from *Pope and Fry* [1997]. Expressions for $a_\phi(\lambda)$, $a_d(\lambda)$, and $a_g(\lambda)$ need to be developed.

The shape of the $a_\phi(\lambda)$ spectrum for a given bio-optical domain can change owing to the pigment-package effect (i.e., the flattening of absorption peaks with increasing intracellular pigment concentration due to self-shading [*Morel and Bricaud*, 1981]) and changes in pigment composition. For a given domain, normalizing measured $a_\phi(\lambda)$ curves to $a_\phi(675)$ reduces the dynamic range and results in a smooth variation for $a_\phi(\lambda)/a_\phi(675)$ versus $a_\phi(675)$ for the MODIS wave bands centered at λ = 412, 443, 488, 531, and 551 nm (e.g., see Figure 3, data for two high-light, subtropical regimes).

$$a_\varphi(\lambda) = a_0(\lambda)\exp\left[a_1(\lambda)\tanh\left[a_2(\lambda)\ln\left(a_\varphi(675)/a_3(\lambda)\right)\right]\right]\bullet a_\varphi(675) \quad (8)$$

A hyperbolic tangent function was chosen to model this relationship in order to ensure that the value of $a_\phi(\lambda)/a_\phi(675)$ approaches an asymptote at very high or very low values of $a_\phi(675)$. *Carder et al.* [1991] detail the behavior of this function with parameterization, although we have substituted $a_\phi(675)$ for the [chl *a*] found in their expression. Using logarithmic scaling for both axes results in the following model equation for $a_\phi(\lambda)$ as a function of $a_\phi(675)$:

where the parameters $a_0(\lambda)$ to $a_3(\lambda)$ are empirically determined for each MODIS wavelength of interest. Here $a_0(\lambda)$ is the most important of the parameters, as it is directly proportional to $a_\phi(\lambda)$.

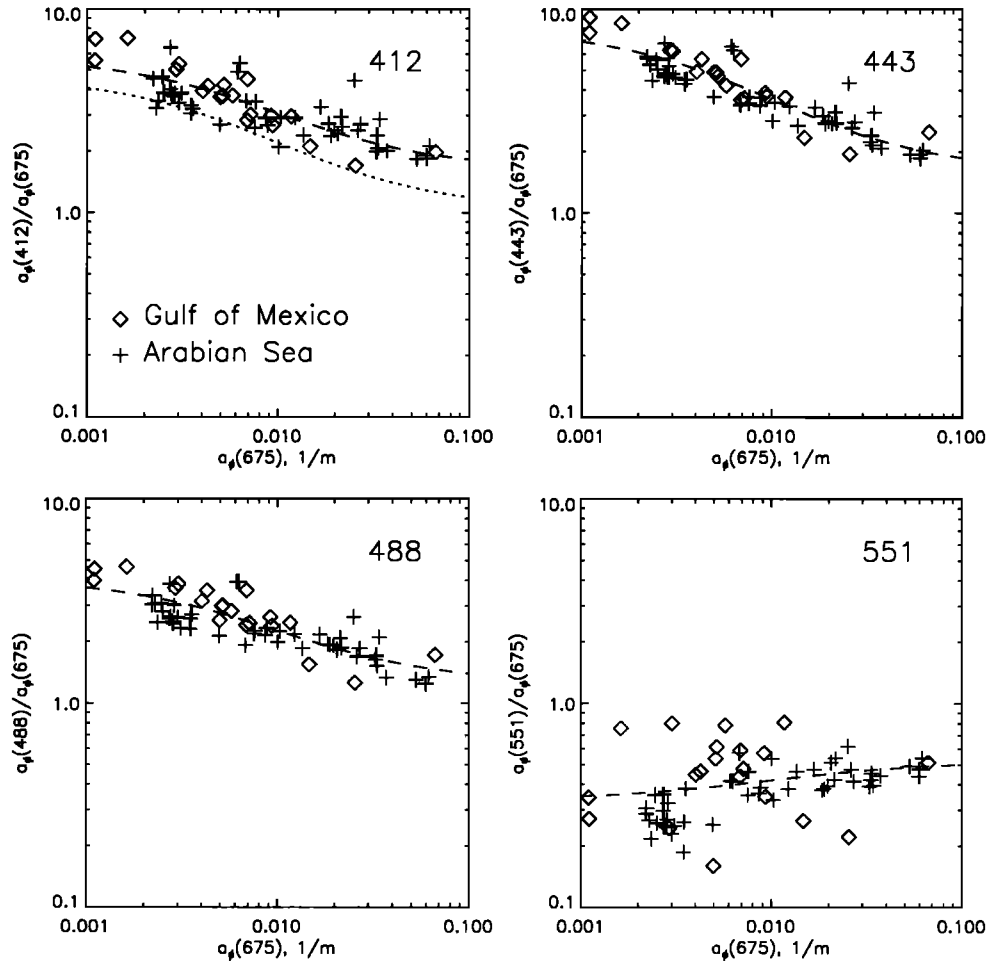

Figure 3. Absorption coefficients $a_\phi(\lambda)/a_\phi(675)$ versus $a_\phi(675)$ for each Moderate-Resolution Imaging Spectrometer (MODIS) ocean wave band. The number at top right corner indicates wavelength λ. The lines are described by equation (8) using the parameters listed in Table 1, and they represent the minimum sum of squared errors for modeled versus measured values of $a_\phi(\lambda)/a_\phi(675)$.

Table 1a. Wavelength-Dependent Parameters for the Semianalytical Chlorophyll Algorithm for Regions Without Packaged Pigments

	Wavelength				
	412	443	488	510	551
b_{bw} (m^{-1})	0.003341	0.002406	0.001563	0.001313	0.000929
a_w (m^{-1})	0.00480	0.00742	0.01632	0.03181	0.05910
a_0	2.20	3.59	2.27	1.40	0.42
a_1	0.75	0.80	0.59	0.35	-0.22
a_2	-0.5	-0.5	-0.5	-0.5	-0.5
a_3	0.0112	0.0112	0.0112	0.0112	0.0112

See text for variable descriptions.

For simplicity, only $a_0(\lambda)$ and $a_1(\lambda)$ are varied to parameterize $a_\phi(\lambda)$, with $a_2(\lambda)$ and $a_3(\lambda)$ being set to the constant values of -0.5 and 0.010, respectively. Figure 3 shows the measured data and the modeled curves for $a_\phi(\lambda)$ measurements taken from the GOMEX, COLOR, and TN048 cruises, all considered to be part of the same high-light, subtropical domain (note that TN048 was an expedition to the Arabian Sea during monsoon conditions). The parameters $a_0(\lambda)$-$a_3(\lambda)$ are listed in Tables 1a and 1b.

The $a_d(\lambda)$ and $a_g(\lambda)$ can both be fit to a curve of the form $a_x(\lambda) = a_x(400) \exp[-S_x(\lambda-400)]$ where the subscript x refers to either d or g [*Bricaud et al.*, 1981; *Roesler et al.*, 1989; *Carder et al.*, 1991]. Owing to this similarity in spectral shape, these terms cannot be spectrally separated with the MODIS channels, so the $a_d(\lambda)$ term is combined operationally with $a_g(\lambda)$, and both detrital and CDOM absorption are represented by $a_g(\lambda)$. The combined CDOM and detritus absorption term is thus written

$$a_g(\lambda) = a_g(400) \exp^{-S(\lambda-400)} \quad (9)$$

Table 1b. Wavelength-Independent Parameters for the Semianalytical Chlorophyll Algorithm for Regions Without Packaged Pigments

Parameter	Value
X_0	-0.00182
X_1	2.058
Y_0	-1.13
Y_1	2.57
S	0.0225
p_0	51.9
p_1	1.00
c_0	0.2818
c_1	-2.783
c_2	1.863
c_3	-2.387

where S is empirically determined. Many researchers have reported that $S_d = 0.011$ nm^{-1}, on average [*Roesler et al.*, 1989]. For the GOMEX and COLOR cruises an average value of 0.017 nm^{-1} was measured for S_g. Values reported by F. Hoge (personal communication, 1998) for the Sargasso Sea were somewhat higher as are those found near swampy regions of the Gulf of Mexico. The algorithm performance was optimized by varying S_g, with the value 0.022 nm^{-1} providing the smallest residual error compared to field measurements. The increase in S is thought to account in part for the lack of gelbstoff fluorescence in the algorithm, which increases $L_w(443)$ relative to $L_w(412)$ [e.g., see *Mobley*, 1994]. Water Raman scattering would also be larger at 443 nm than at 412 nm, but it is very small and is quenched by increasing gelbstoff absorption at the ultraviolet excitation wavelengths [*Mobley*, 1994].

As a final note on the R_{rs} model, (5) - (9) are written in a general way to emphasize that the values of the parameters X_0, X_1, Y_0, Y_1, a_0, a_1, and S are not meant to be absolute. They should be updated and changed as more data become available. These parameters may also be changed with region and season to optimize algorithm performance.

3.4. Inverting the Model

All of the pieces of the reflectance model are now in place. Via (2)-(4), and (5)-(9), $R_{rs}(\lambda)$ can be expressed solely as a function of the "constant" term, $R_{rs}(443)$, $R_{rs}(488)$, $R_{rs}(551)$, $a_\phi(675)$, and $a_g(400)$, given values for the parameters for X_0, X_1, Y_0, Y_1, $a_0(\lambda)$, $a_1(\lambda)$, and S. $L_w(\lambda)$ from MODIS can be converted into $R_{rs}(\lambda)$ as mentioned previously. Then, for each pixel, the R_{rs} model equation can be written for each of the five visible MODIS ocean wave bands, yielding five equations written in three unknowns: the constant term, $a_\phi(675)$, and $a_g(400)$.

Using spectral ratios of R_{rs} eliminates the constant term, since it is largely independent of wavelength. In principle, two spectral ratio equations can be used to solve for the two remaining unknowns, $a_\phi(675)$ and $a_g(400)$. On the basis of the shape of the absorption curve for phytoplankton versus those for CDOM and detritus, equations using spectral ratios of 412:443 and 443:551 for $R_{rs}(\lambda)$ should provide a good separation of the two absorption contributions. Our two equations are

The right-hand side of each equation is a function of $a_\phi(675)$, $a_g(400)$, $R_{rs}(443)$, $R_{rs}(488)$, and $R_{rs}(551)$. Since the R_{rs} values are provided on input, we now have two equations in two unknowns. The equations can usually be solved algebraically to provide values for $a_\phi(675)$ and $a_g(400)$. The computational method of solving these equations is described in section 3.9.

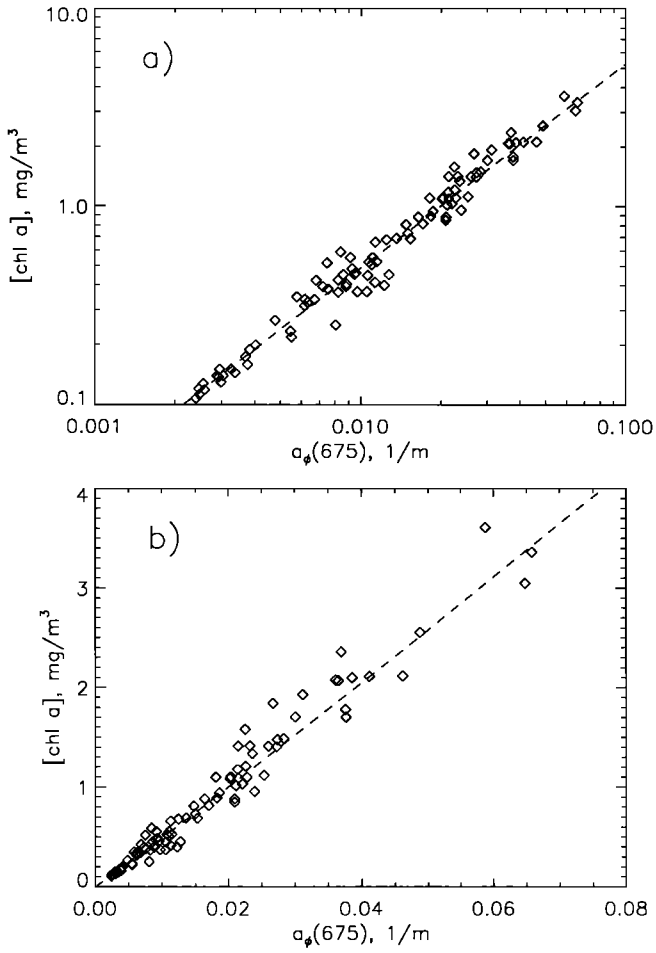

Figure 4. The [chl *a*] versus $a_\phi(675)$ in (a) logarithmic scaling and (b) normal scaling. In both charts the dashed line is the equation $[\text{chl } a] = 56.8[a_\phi(675)]^{1.03}$, which is the result of linear regression on the log-transformed values ($n = 96$, $r^2 = 0.97$).

$$\frac{R_{rs}(412)}{R_{rs}(443)} = \frac{b_b(412)}{b_b(443)}\,\frac{a(443)}{a(412)}$$
$$\frac{R_{rs}(443)}{R_{rs}(551)} = \frac{b_b(443)}{b_b(551)}\,\frac{a(551)}{a(443)} \qquad (10)$$

For waters with high concentrations of CDOM and chlorophyll, $L_w(412)$ and $L_w(443)$ values are small and the semi analytical algorithm cannot perform properly. It is thus designed to return values only when modeled $a_\phi(675)$ is less than 0.03 m^{-1}, which is equivalent to [chl *a*] of about 1.5–2.0 mg m^{-3}. Otherwise, an empirical algorithm for [chl *a*] is used, which is described in section 3.6.

3.5. Chlorophyll *a* Algorithm for Semianalytical Case

When the semianalytical algorithm returns a value for $a_\phi(675)$, [chl *a*] is determined via a direct relationship to this value. This step requires knowledge of the chlorophyll-specific absorption coefficient for phytoplankton at 675 nm, $a_\phi^*(675)$, for the bio-optical domain involved. *Bricaud et al.* [1995] demonstrated a wide range of values for $a_\phi^*(675)$ using a global data set. If only surface values for waters in a more limited bio-optical domain (e.g., tropical and subtropical waters) are examined, however, this variability is greatly reduced. Phytoplankton found in high-light environments, for example, have relatively low concentrations of light-harvesting accessory pigments and relatively high concentrations of photoprotective pigments compared to plants found in samples from high latitudes, upwelling centers, or deep in the euphotic zone. Therefore the effects of accessory pigment absorption on the variability of the largely chlorophyll *a* dominated red peak at 675 nm are small in high-light environments. Furthermore, photoprotective pigments do not absorb light at 675 nm, and so they do not affect $a_\phi(675)$, even if they are present in large quantities.

$$[chl\ a] = P_0\ [a_\phi(675)]^{P_1} \qquad (11)$$

To evaluate variations of $a_\phi(675)$ with [chl *a*] for subtropical to tropical waters, we developed a data set to explore the more limited variation in surface values of $a_\phi^*(675)$ under high-light conditions (see section 4.2.1 for methodology). This data set came from surface-water samples from several cruises in the Gulf of Mexico (BONG 1, BONG 2, BOSS 1, and WFS) and one cruise to the Arabian Sea (TN048). Linear regression of log([chl *a*]) versus log[$a_\phi(675)$] yielded an equation of the form

For the data set mentioned above, the regression resulted in p_0 and p_1 values of 56.8 and 1.03, respectively ($n = 95$, $r^2 = 0.97$ on the log-transformed values). This regression and the data are shown in Figure 4. Within a given bio-optical domain, we find only a very weak change in $a_\phi^*(675)$ with [chl *a*]. The exponent is close enough to 1.0 that little error occurs by linearizing the parameter values to 51.9 and 1.00, respectively, for that domain. This suggests an average $a_\phi^*(675)$ value of 0.0193 m^2 (mg chl)$^{-1}$ for subtropical data sets.

3.6. Pigment Algorithm for Default Case

When the semi analytical algorithm does not return a value for $a_\phi(675)$ owing to low values of $R_{rs}(412)$ in eutrophic waters, we provide an empirical, two-wavelength algorithm for [chl *a*] to use by default. *Aiken et al.* [1995] found that the $L_w(488)/L_w(551)$ ratio (or nearby wavelengths) is best for empirical [chl *a*] determination. We use an equation of the form

$$\log\ [chl\ a]_{emp} = c_0 + c_1\log(r_{35}) + c_2[\log(r_{35})]^2 + c_3[\log(r_{35})]^3 \qquad (12)$$

where

$$r_{35} = \frac{R_{rs}(488)}{R_{rs}(551)} \qquad (13)$$

$[\text{chl } a]_{emp}$ is called the "empirical" or "default" chlorophyll *a* concentration, and c_0, c_1, c_2, and c_3 are empirically derived constants.

A subtropical and temperate summer data set was constructed from stations from the MLML 2, GOMEX, COLOR, and TN042 cruises and from stations below 45°N from the TT010 cruise (Table 2). This data set includes both open-ocean and riverine-influenced stations. A quadratic regression of log([chl *a*]) against $\log(r_{35})$ for measured [chl *a*] and $R_{rs}(\lambda)$ for this data set yielded a root-mean-square (RMS) error of 0.51. The data and the regression line are shown in Figure 5. With the addition of more low-chlorophyll data points from near Hawaii, the Kuroshio, and the equatorial Pacific (see section 4.3.1), however, an extended tropical and subtropical data set including more low-pigment stations was better fit empirically using a cubic regression equation in logarithmic units, with the coefficients shown in Tables 1a and 1b.

3.7. Weighted Pigment Algorithm

Another consideration is that there should be a smooth transition in [chl *a*] values when the algorithm switches from the

Table 2. Cruises With Optical and Bio-optical Data Collected by the University of South Florida (Carder Data Set) for Initial Tests of the Unpackaged Algorithm

Cruise	Start Date	End Date	Region	Number of Stations
MLML 2	Aug. 13, 1991	Aug. 29, 1991	North Atlantic, 42°N–60°N	7
TT010	July 20, 1992	Aug. 2, 1992	North Pacific, 24°N–48°N	10
GOMEX	April 10, 1993	April 19, 1993	northern Gulf of Mexico	21
COLOR	May 31, 1993	June 9, 1993	northern Gulf of Mexico	13
TN042	Nov. 29, 1994	Dec. 18, 1994	Arabian Sea	12
TN048	June 21, 1995	July 13, 1995	Arabian Sea	41

Total number of stations is 104.

semianalytical to the empirical method. For case 1 waters and less extreme solar zenith angles, the semi analytical and empirical algorithm perform reasonably consistently (e.g., Figure 6). From space, however, one can imagine times when high solar zenith angles and high CDOM will combine to reduce the signal-to-noise ratio (SNR) at 412 and 443 nm such that the semianalytic algorithm will have substandard performance. Similarly, high CDOM will degrade the performance of the empirical algorithm. This could result in a step-like transition in the chlorophyll image, which smoothing will mitigate (note that the code has a flag indicating when low-SNR data points arise).

This smoothing is achieved by using a weighted average of the [chl *a*] values returned by the two algorithms when near the transition border. When the semianalytical algorithm returns an $a_\phi(675)$ value between 0.015 and 0.03 m^{-1}, [chl *a*] is calculated as

$$[chl\ a] = w\ [chl\ a]_{sa} + (1 - w)[chl\ a]_{emp} \qquad (14)$$

where $[chl\ a]_{sa}$ is the semianalytically derived value and $[chl\ a]_{emp}$ is the empirically derived value and the weighting factor is $w = [0.03 - a_\phi(675)]/0.015$. The weighting factor is simply a linear function, and this approach is tested later with a global data set.

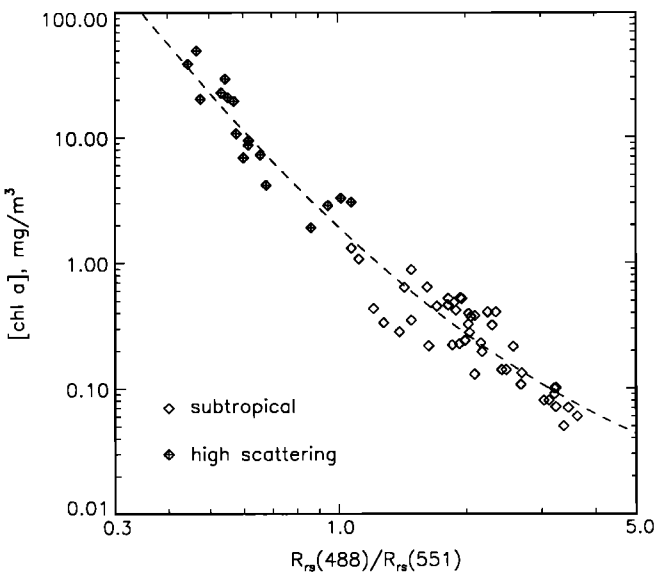

Figure 5. The [chl *a*] versus $R_{rs}(488)/R_{rs}(551)$ in log-log scaling. The dashed line represents a quadratic regression on the log-transformed value and describes the default [chl *a*] algorithm.

3.8. Total and Phytoplankton Absorption Coefficients

The phytoplankton absorption coefficients $a_\phi(\lambda_i)$ are calculated by inserting the modeled $a_\phi(675)$ value into (8) and by using the necessary parameters from Tables 1a and 16 for each wavelength. The total absorption coefficients $a(\lambda_i)$ are calculated by inserting the modeled $a_g(400)$ value and the S parameter from Tables 1a and 1b into (9) to get $a_g(\lambda_i)$ and then combining the result with the $a_\phi(\lambda_i)$ and $a_w(\lambda_i)$ values using (7) and Tables 1a and 1b, respectively.

3.9. Numerical Computation

Here $a_\phi(675)$ and $a_g(400)$ are determined from (10) with the substitutions discussed in section 3.4. Inverting one of the equations to isolate $a_g(400)$ and substituting into the other equation, all terms are then moved to one side. This yields a function that depends only on $a_\phi(675)$ (given values for R_{rs} and the algorithm parameters from Tables 1a and 1b). The value of $a_\phi(675)$ at which the function crosses zero is the solution we seek. This solution is determined computationally via the bisection method. A 33-element array of $a_\phi(675)$ values, scaled logarithmically from 0.0001 to 0.03 m^{-1} is created, and the function is evaluated at the two extremes. If the function changes sign between the two outermost values, a solution exists on the $a_\phi(675)$ interval. The function is then evaluated at the midpoint of the array, and the half in which the function changes sign becomes the new search interval. In this manner the solution interval, which will be two adjacent points on the $a_\phi(675)$ array, is determined in five iterations. Linear interpolation across the interval yields the semianalytical $a_\phi(675)$ value, and $a_g(400)$ is determined via either one of the ratio equations (equation (10)) using the modeled value of $a_\phi(675)$. If the function does not change sign across the two outermost values, a solution cannot be obtained and a switch is made to the empirical, two-wavelength, default algorithm.

When compared to an older method (look-up tables [*Carder et al.*, 1991]), the bisection method gave identical solutions to within five significant digits for $a_\phi(675)$ and $a_g(400)$, and the code ran in 75% of the time that the version of the code based on the look-up table required.

The algorithm code is written in American National Standards Institute (ANSI) C. The program file contains about 300 lines of code and comments. It was developed and tested on a DEC Alpha machine. It was also tested on Silicon Graphics, SUN, and PC machines. All of the algorithm parameters listed in Tables 1a and 1b are read in from a file, so different parameter tables can easily be constructed for different applications (see below). The code is available upon request.

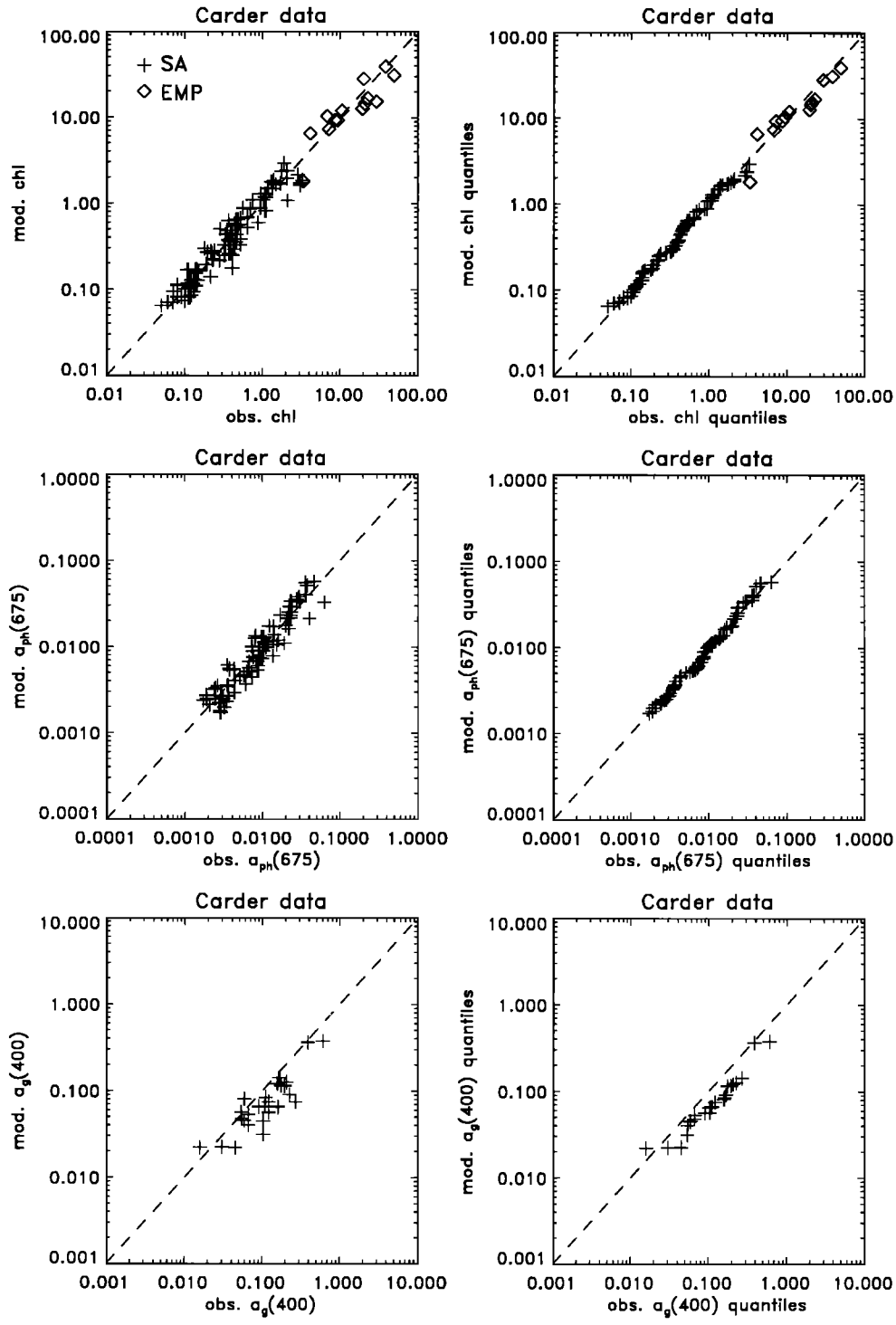

Figure 6. Algorithm performance for Carder data set, top observed versus modeled chl *a*, middle observed versus modeled $a_{ph}(675)$, and bottom observed versus modeled $a_g(400)$ in left scatterplots and right quantile-quantile plots. The lines are the one-to-one lines, SA (crosses) indicates points that are calculated semianalytically or by a blend of semianalytical and empirical values, while EMP (diamonds) indicates points that are calculated empirically.

4. Measurements

4.1. Statistical Criteria

To evaluate algorithm performance, we generated statistics that are determined on log-transformed variables so as to provide equal weight to data from all parts of the pigment and reflectance ranges. The slope and intercept values are from type II RMA regressions. The RMS statistic described is based on the root-mean-square of the logarithm of the ratio of modeled-to-measured values [*O'Reilly et al.*, 1998] and will be referred to here as RMS1. We also generated values for r^2 and root-mean-square error on the non-log-transformed (linear) data. This statistic will be referred to as RMS2 and is described by

$$RMS2 = \sqrt{\frac{\sum_{i=1}^{n}\left[\frac{x_{\mathrm{mod},i} - x_{obs,i}}{x_{obs,i}}\right]^2}{n - 2}} \quad (15)$$

where $x_{\mathrm{mod},i}$ is the modeled value of the ith element, $x_{\mathrm{obs},i}$ is the observed (or in situ or measured) value of the ith element, and n is the number of elements. Note that 10^{RMS1}-1.0 ≈ RMS2 if there is no bias between the modeled and measured data. We used two graphical means of evaluating algorithm performance, scatterplots of modeled versus observed values and quantile-quantile plots [*O'Reilly et al.*, 1998].

4.2. Tests With University of South Florida Data

4.2.1. Methods. We initially tested our algorithm with our own subtropical and temperate-summer data set, called the Carder data set (Table 2), since observed values of $a_\phi(675)$ and $a_g(400)$ are included wherever possible to accompany the observed $R_{rs}(\lambda)$ and [chl *a*] values. Also, 17 points from high-chlorophyll, high-scattering stations, mostly from the extended Mississippi River Plume region, are included. We later test the algorithm with global $R_{rs}(\lambda)$ and [chl *a*] data collected by international research teams and found in the NASA SeaBASS data archive.

$R_{rs}(412)$, $R_{rs}(443)$, $R_{rs}(488)$, $R_{rs}(531)$, and $R_{rs}(551)$ for the Carder data set were derived from hyperspectral $R_{rs}(\lambda)$ measurements collected just above the sea surface (for measurement protocols, see *Lee et al.*, [1996]) by weighting to simulate the MODIS band responses [*Barnes et al.*, 1994]. Most $R_{rs}(\lambda)$ measurements in the SeaBASS global database were collected from just below the sea surface following the protocols of *Mueller and Austin* [1995]. Both data types are combined in algorithm performance tests against the global data.

All [chl *a*] values were determined fluorometrically [*Holm-Hansen and Riemann*, 1978; *Mueller and Austin*, 1995]. The $a_g(400)$ was determined by measuring seawater filtered through a 0.2 μm pore-sized nylon filter in a spectrophotometer when compared to a MilliQ water blank [*Mueller and Austin*, 1995].

The method used to determine absorption coefficients for particles and for detritus involves filtering as much as 4 L of water through a 25 mm diameter, Whatman glass fiber filter (GFF). The protocols used are those discussed in *Mueller and Austin* [1995] and are based on methods developed by *Shibata* [1958], *Roesler et al.* [1989], *Mitchell* [1990], *Nelson and Robertson* [1993], and *Moore et al.* [1995]. In order to estimate absorption coefficients from the OD measurements, an optical path-elongation factor, called β, which is dependent upon OD, is employed. Recently, however, it has been shown that β varies with the particle size prevalent to a region [*Moore et al.*, 1995]. This happens because smaller particles get more deeply embedded into the pad, providing a greater absorption cross section for photons scattered back and forth across the particle substrate than do the large particles remaining at the surface of the pad. For our work we chose a β factor appropriate for small, subtropical particles that falls between two published β factors, one developed for detritus [*Nelson and Robertson*, 1993] and one for synechococcus [*Moore et al.*, 1995]. Our β factor is

$$\beta = 1.0 + 0.6\,OD^{-0.5} \quad (16)$$

Furthermore, we loaded the filter pads enough that the pad optical density exceeded 0.04 at 675 nm [*Bissett et al.*, 1997] for more accuracy in $a_\phi(\lambda)$ measurements.

4.2.2. Results. The algorithm parameters used are shown in Tables 1a and 1b. [chl *a*], $a_\phi(675)$, and $a_g(400)$ values were predicted by the semianalytical algorithm with RMS1 errors of 0.122, 0.131, and 0.252, respectively, and with RMS2 errors of 0.289, 0.302, and 0.405, respectively (Table 4), for a largely subtropical or temperate-summer data set.

The results are also shown as scatter and quantile plots (Figure 6). The crosses on the plots are the points determined with the semianalytical portion of the blended algorithm, and the diamonds represent points determined with the default or empirical algorithm. The high-chlorophyll points extend nicely along the one-to-one line on both the scatter and quantile plots. The RMS1 and RMS2 errors for [chl *a*] for this composite data set (n=104) were 0.132 and 0.300, respectively.

Since the default portion of the algorithm does not yet return values for $a_\phi(675)$ and $a_g(400)$, these variables can not be shown for eutrophic data. An empirical expression for $a_\phi(\lambda)$ and $a_g(\lambda)$ has been developed by *Lee et al.* [1998] and will be incorporated later into the algorithm.

The [chl *a*] and $a_\phi(675)$ data appear to be quite evenly clustered about the one-to-one line on both scatter and quantile plots with no aberrant tails at either end. The $a_g(400)$ points are predominantly below the one-to-one line and show a low bias. There are only 26 points in this plot because measured values of $a_g(400)$ are infrequently available for comparison. These data were subtropical except for some late-summer, temperate data, and they had relatively large specific absorption coefficients. Thus they are representative of the domain we designated as unpackaged.

4.3. Tests Using a Global Data Set

4.3.1. Data set. A large (n=919) global evaluation data set consisting of measured R_{rs} values at the Sea-viewing Wide-field-of-view Sensor (SeaWiFS) wavelengths and chlorophyll *a* measurements based on both fluorometric and high-performance liquid chromatography (HPLC) methods was archived by the NASA SeaWiFS Project as the SeaBAM data set [*O'Reilly et al.*, 1998]. These data came from various researchers around the United States and Europe and contain mostly subsurface R_{rs} values. In addition to these data, we have received 36 data points from the equatorial Pacific, consisting of R_{rs} measurements made above the surface (EqPac, courtesy of C. Davis), and we collected additional above-water data sets from the Southern California Bight (SCB) (April 1997 with G. Mitchell), near Hawaii (February 1997 with D. Clark), and the Kuroshio edge of the East China Sea (May 1997 with G. Gong), which we have added to the global data set. This combination of 976 data points allows for algorithm comparisons using a data set consisting of both above-water and below-water points.

The recent SCB data set provided an opportunity to compare above-water R_{rs} data with the historical California Cooperative Oceanic Fisheries Investigations (CalCoFI) SCB subsurface R_{rs} data set from the SCB. We also measured phytoplankton absorption spectra in the SCB in late winter to adjust $a_\phi(\lambda)$ curve parameters, providing a more "packaged" parameterization (Table 3) for modeling the multiyear CalCOFI data set of subsurface R_{rs} values and similar eastern boundary environments.

4.3.2. Numerical filters. Since many different locations and sensors were involved in compiling the SeaBASS data collections and as many as eight separate upwelling and downwelling sensor channels must be well calibrated to provide accurate spectral ratios of R_{rs} for the semianalytical algorithm, an attempt was made to select an initial core set of data consistent with case 1 waters and with each other. Also, an attempt was made to partition the data sets into two regions, ones where little pigment packaging is to be expected (e.g., high-light, nonupwelling locations in warm, tropical and subtropical waters) and one where more packaging

Table 3. Algorithm Parameters Used With the Packaged and Modified Global Data Sets

Parameter	Packaged	Global
$a_0(412)$	1.90	1.95
$a_0(443)$	2.70	2.95
$a_0(488)$	1.90	1.99
$a_2(\lambda)$	-0.45	-0.5
$a_3(\lambda)$	0.021	0.025
p_0	74.1	72.4
p_1	1.0	1.0
p_2	0.0	0.0
c_0	0.4818	0.3147
c_1	-2.783	-2.859
c_2	1.863	2.007
c_3	-2.387	-1.730

All algorithm parameters not listed here are the same as in Tables 1b. The values of $a_3(\lambda)$ shown apply to all of the Moderate-Resolution Imaging Spectrometer (MODIS) wavelengths. The equation to determine chl *a* from $a_\phi(675)$ for this data set is given by (11).

might be expected (e.g., eastern boundary upwelling, and nonsummer high-latitude data). To assist in this task, each SeaBASS data set was individually examined.

Some of the data sets were composed of data largely falling into a single type of bio-optical domain according to the numerical filters discussed below. Others spanned two or more domains. Data sets falling primarily into the domain where the pigments appeared to be relatively unpackaged with significant photoprotective pigments [e.g., high $a_\phi^*(443)$ and high $a_\phi(443)/a_\phi(675)$] were first tested using the semianalytical algorithm with the parameters shown in Tables 1a and 1b.

The first numerical filter compares the data sets to the historic [*Gordon et al.*, 1983] CZCS chlorophyll pigment algorithm [Chl $a = 1.14\,[r_{25}]^{-1.71}$, $r_{25} = R_{rs}(443)/R_{rs}(550)$] to check for consistency with this classical algorithm for case 1 waters with relatively little packaging. Figures 7d, 8d, and 9d show scatterplots of observed [chl *a*] versus r_{25} for different sets of warm-water data, with the CZCS algorithm illustrated by the dotted line. The warm-water, subtropical and tropical data sets, with little in the way of pigment packaging and probably high photoprotective to chlorophyll ratios (Figure 7d), were found to be centered over the CZCS algorithm for pigment values less than about 1 mg m^{-3}.

When the CZCS algorithm was applied to data from high-latitude or eastern boundary upwelling locations where pigments are packaged into larger cells with more self-shading (Figure 8d), however, the CZCS-like chlorophyll *a* values were typically 50%

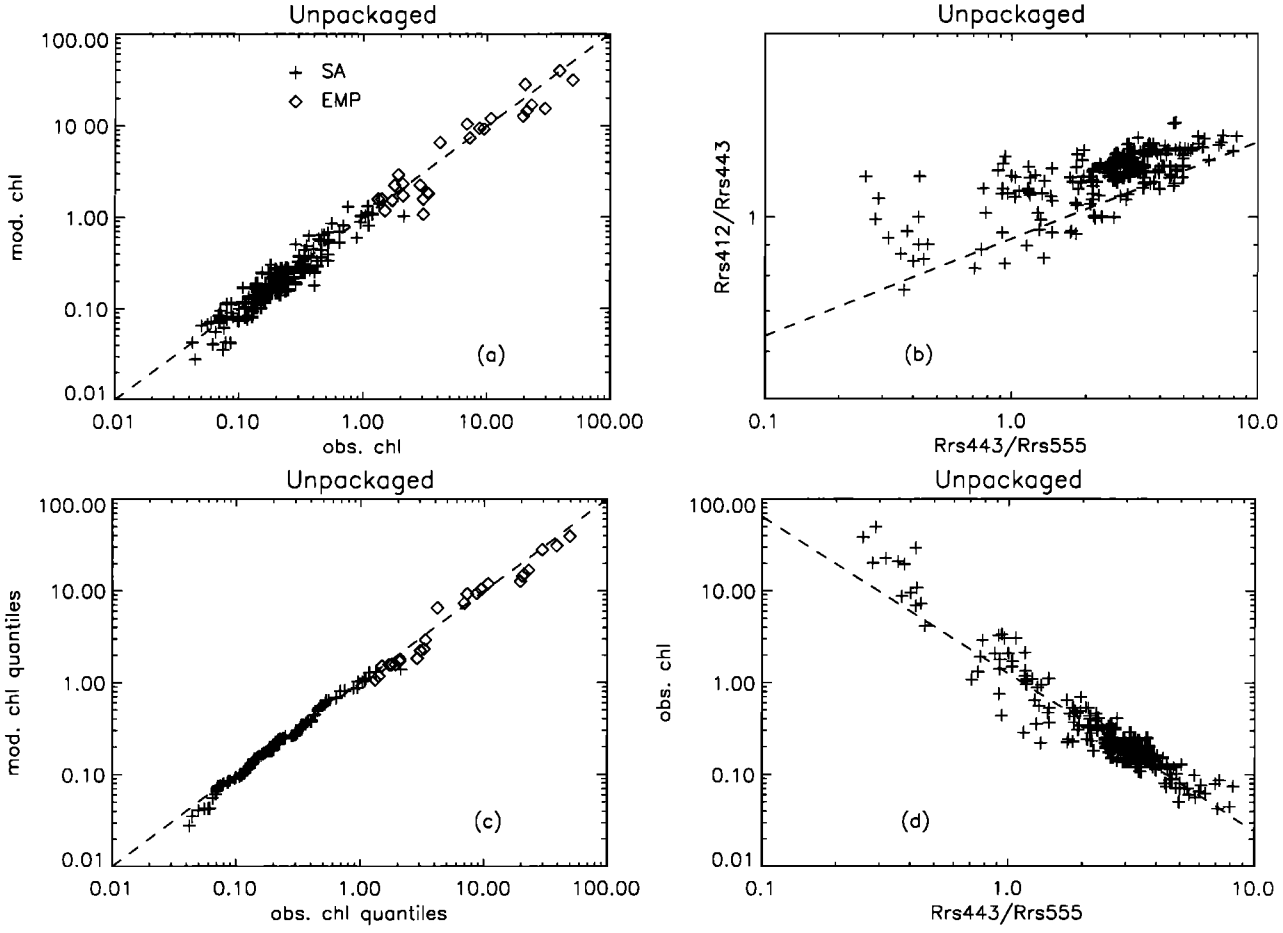

Figure 7. Algorithm performance for and analysis of data sets passing the "unpackaged" numerical filter. (a) Scatterplot of observed versus modeled chl *a* (mg m^{-3}). The dashed line is the one-to-one line. (b) The r_{12} versus r_{25}, with the line, $r_{12} = 0.95[r_{25}]^{0.16}$, used to identify "unpackaged" case 1 data (above line). (c) Quantile-quantile plot of observed versus modeled chl *a*. (d) Observed chl *a* versus r_{25}, with the Coastal Zone Color Scanner (CZCS) algorithm line $C = 1.14[r_{25}]^{-1.71}$.

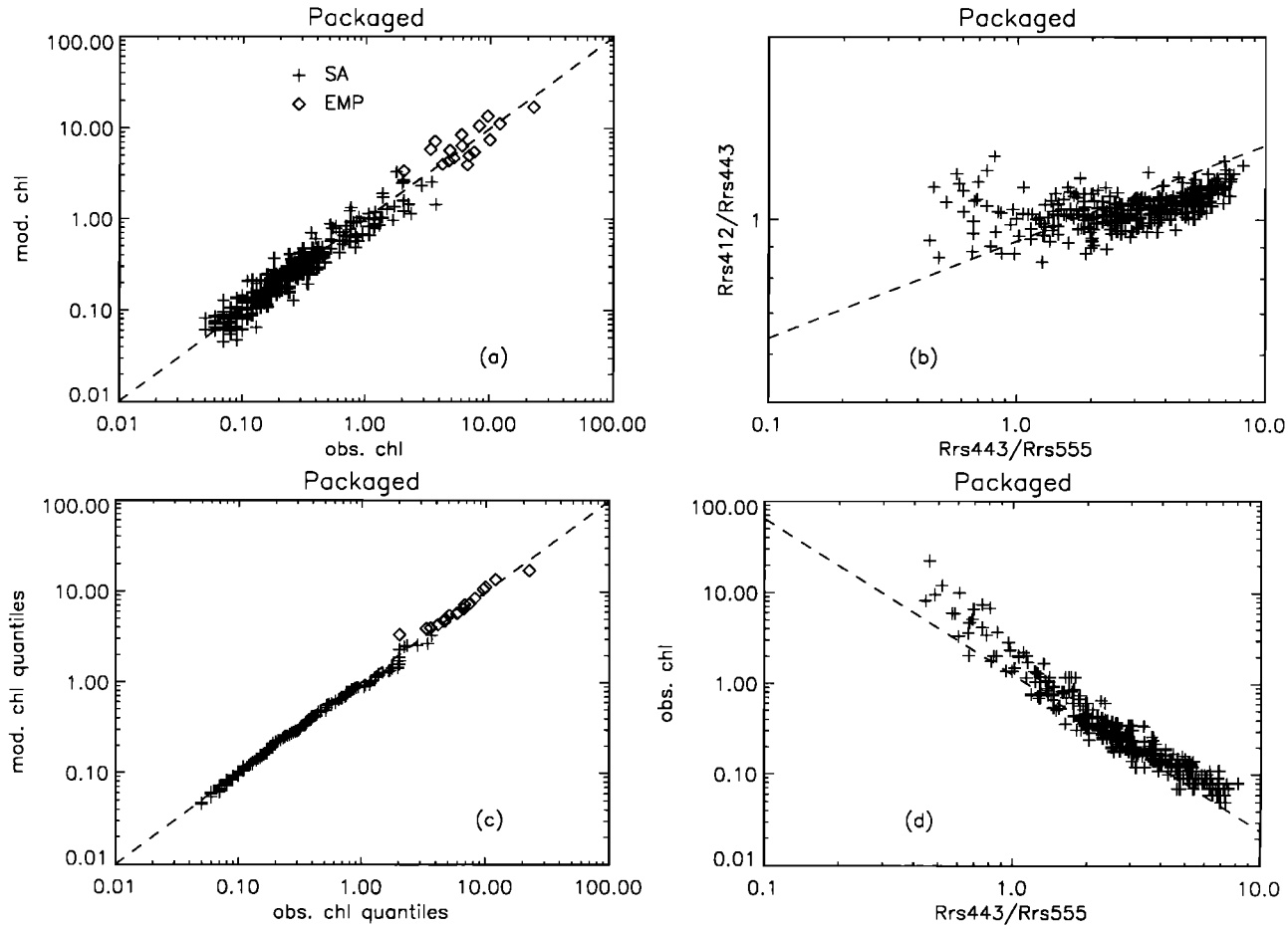

Figure 8. Algorithm performance for and analysis of data sets passing the "packaged" numerical filter. (a) Scatterplot of observed versus modeled chl *a* (mg m^{-3}). The dashed line is the one-to-one line. (b) The r_{12} versus r_{25}, with the line, $r_{12} = 0.95[r_{25}]^{0.16}$, used to identify "unpackaged" case 1 data (above line). (c) Quantile-quantile plot of observed versus modeled chl *a*. (d) Observed chl *a* versus r_{25}, with the Coastal Zone Color Scanner (CZCS) algorithm line $C = 1.14[r_{25}]^{-1.71}$.

to 90% lower than those measured. This effect of differing bio-optional domains on the performance of the CZCS-like algorithm suggests that regional algorithms are needed to obtain best results for different regions or seasons as suggested by *Mitchell and Holm-Hansen* [1991].

This "filter" approach helped us separate various data sets into two domains, which we call the unpackaged-pigment domain and packaged-pigment domain. This type of domain-selection filter, however, cannot be applied to satellite-derived data because of the need for measurements of [chl *a*]. Thus a second type of numerical filter was sought that was reliant on only space-derived data.

The second numerical filter uses the ratios r_{12} [= $R_{rs}(412)/R_{rs}(443)$] and r_{25} (Figures 7b, 8b, and 9b) and is applicable to satellite-derived data. For the Carder data set the line $r_{12} = 0.95\ [r_{25}]^{0.16}$ was used to separate high-gelbstoff data points (those below the line in Figure 7b) from the case 1 data. On the basis of the Carder a_g data, the gelbstoff-rich case 2 data had $a_g(400)$ values typically in excess of the relationship $0.12\ [\text{chl } a]^{0.7}$ or $a_g(443) > a_\phi(443)$. This line also separates case 1 data representative of more packaged domains from those representative of less packaged domains since the ratio r_{12} is less affected by packaging effects than is r_{25}. Thus, for waters far from terrigenous influences, the second filter provides a flag for packaging effects.

Case 1 waters with more packaged pigments from a traditional upwelling region (e.g., CalCOFI) were also examined using the second numerical filter. These data fell mostly below the filter line (Figure 8b) in comparison to the unpackaged data, which fell mostly above the line (Figure 7b). Since pigment packaging reduces the absorption for a given concentration of pigments far more at 443 than at 551 nm, and somewhat more at 443 than at 412 nm [*Morel and Bricaud*, 1981], packaging and reduction of photoprotective pigments significantly increases r_{25} while increasing the r_{12} ratio somewhat. This places packaged data points below the $r_{12} = 0.95\ [r_{25}]^{0.16}$ line (Figure 8b) even without excessive gelbstoff concentrations, at least for points with r_{25} values in excess of a value of about 3.0. Filter 2, then, provides a space-based method for separating data points with packaged pigments from those with unpackaged pigments, at least for the oligotrophic end of the data sets.

Filter 2, however, can be distorted by a poorly calibrated sensor or by inaccurate atmospheric correction, so it is inadvisable to use it exclusively as a packaging filter without some means of providing an independent check on its performance. A means of accomplishing this task is found in section 5.

4.4. Algorithm Evaluation With "Unpackaged" Data Set

Those data sets generally found to be consistent with the CZCS algorithm line and which were located primarily above the line $r_{12} = 0.95\ [r_{25}]^{0.16}$ for points where $r_{25} > 3.0$, were numerically

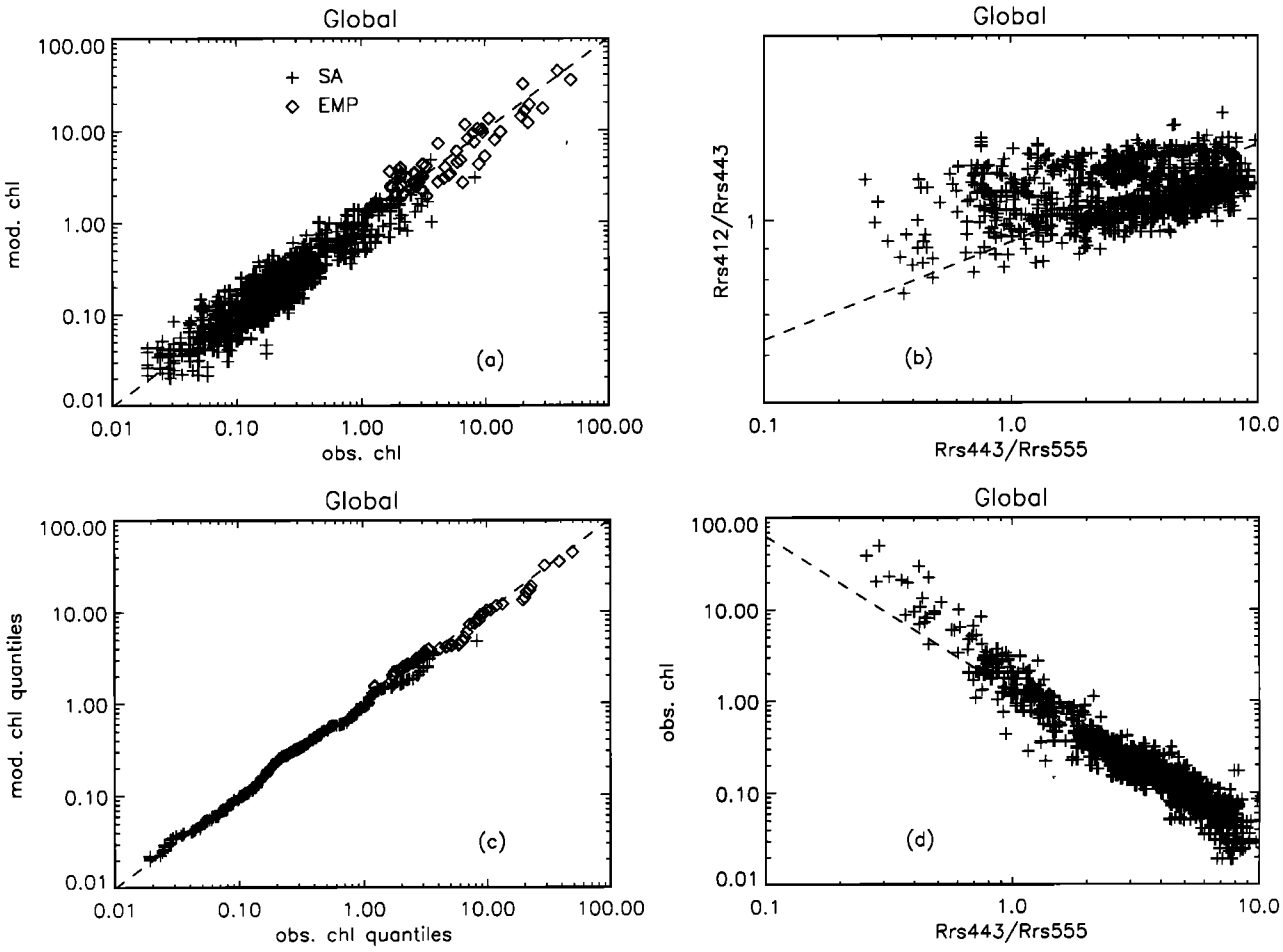

Figure 9. Algorithm performance for and analysis of global data sets without partitioning into "packaged" or "unpackaged" subsets. (a) Scatterplot of observed versus modeled chl *a* (mg m^{-3}). The dashed line is the one-to-one line. (b) The r_{12} versus r_{25}, with the line, $r_{12} = 0.95[r_{25}]^{0.16}$, used to identify "unpackaged" case 1 data (above line). (c) Quantile-quantile plot of observed versus modeled chl *a*. (d) Observed chl *a* versus r_{25}, with the Coastal Zone Color Scanner (CZCS) algorithm line $C = 1.14[r_{25}]^{-1.71}$.

classified as unpackaged, in reference to the pigment-absorption effects on the optics prevalent at those locations at the time of data collection. Those data sets with high-r_{25} points largely below the line were classified as packaged, and a test of a packaged algorithm is developed and discussed below. Those data sets with high-r_{25} points fairly equally divided by the line were withheld from the tests of both the unpackaged and packaged algorithm, but they were included as part of the test of a global algorithm developed and discussed below.

There are 287 data points in the unpackaged ensemble data set: 134 USF data points and 37 EqPac, equatorial Pacific points, all measured above water and processed using the *Lee et al.* [1996] protocols, and an additional 126 EqPac points, all measured below the surface using the *Mueller and Austin* [1995] protocols. Of these points, 261 (91%) were processed by the semianalytical portion of the [chl *a*] algorithm, yielding RMS1 and RMS2 errors of 0.099 and 0.230, respectively (Table 4). The scatter (Figure 7a) and quantile (Figure 7c) plots overlay the one-to-one line at the ends as well as in the middle. For the log-transformed variables, the type II RMA slope was 0.999, the bias was 0.002, and the correlation coefficient r^2 was 0.873. When all 287 data points were considered using the semianalytical algorithm plus the blended and empirical algorithms, RMS1 and RMS2 errors were 0.108 and 0.242, respectively. The type II RMA slope was 0.973, the bias was -0.003, and r^2 was 0.955. Note that for this unpackaged data set, the transition from the semi-analytic to the default algorithm is reasonably smooth (Figure 7c).

Table 4 provides a complete summary of these statistics. Note that since these algorithms are largely semianalytical in nature and were developed based mostly upon Gulf of Mexico data for the parameterization, one would not expect to have slope values of 1.000 and bias values of 0.000. Note also that the r^2 values increased using the blended algorithm because of the extended range of chlorophyll *a*. It is important to note that RMS2 errors of less than 25% significantly exceed our accuracy goal of 35% or less.

4.5. Algorithm Evaluation With "Packaged" Data Set

Several data sets within the global evaluation set were numerically diagnosed as coming from waters where the pigments were much more packaged than those from the warm, tropical and subtropical data sets evaluated earlier. The new packaged parameters, shown in Table 3, are used to define a slightly different, packaged algorithm for upwelling and winter-spring temperate regions.

There are 326 points in an ensemble of multiyear, multiseason data sets from the California Current which we label as packaged. These consist of historical CalCOFI (n=303) and recent Cal9704

Table 4. Summary of Regression Statistics for Each Data Set Tested.

Data Set	Variable	n	Intercept	Slope	Bias	r^2	RMS1	RMS2
Carder	chl SA	86	0.019	1.020	0.010	0.921	0.122	0.289
Carder	chl SA+EMP	104	-0.007	0.977	-0.002	0.963	0.132	0.300
Carder	$a_\phi(675)$ SA	82	0.098	1.052	-0.008	0.898	0.131	0.302
Carder	$a_g(400)$ SA	26	-0.278	0.905	-0.186	0.751	0.252	0.405
Unpackaged	chl SA	261	0.001	0.999	0.002	0.873	0.099	0.230
Unpackaged	chl SA+EMP	278	-0.019	0.973	-0.003	0.955	0.108	0.242
Packaged	chl SA	303	-0.006	0.999	-0.006	0.917	0.111	0.268
Packaged	chl SA+EMP	326	0.004	1.012	-0.003	0.951	0.114	0.282
Global	chl SA	883	0.002	1.003	0.002	0.852	0.176	0.446
Global	chl SA+EMP	976	0.003	1.003	0.002	0.913	0.174	0.440

The unpackaged data consists of the Carder, Equatorial Pacific (EqPac) above-surface, EqPac below-surface, Taiwan, and MOCE3 data sets. The packaged data consists of the California Cooperative Ocean Fisheries Investigators (CalCOFI), and CAL9704 data sets. The global data consists of the global evaluation data set, minus the Cota and University of Maryland data plus the high-chlorophyll Carder, EqPac above-surface, Taiwan, and MOCE3 data, and uses one set of average algorithm parameters for the whole data set. Here n is the number of samples and r^2 is the correlation coefficient. SA indicates that only the modeled values that passed the semianalytical portion of the algorithm are used (including blended values). SA+EMP indicates that all modeled values, semianalytical, blended, and empirical, are used. All statistics except RMS2 are calculated from $\log_{10}$-transformed variables.

(n=23) data which we recently collected with G. Mitchell. The CalCOFI R_{rs} data were subsurface measurements, while the Cal9704 data were above-surface collections. Three hundred and three points (93%) from this packaged data set passed the semianalytical portion of the new algorithm, yielding RMS1 and RMS2 errors for [chl *a*] retrieval of 0.111 and 0.268, respectively. The type II RMA slope and intercept was 0.999, the bias was -0.006, and the r^2 value was 0.917. The scatterplot (Figure 8a) overlays the one-to-one line, and the quantile plot (Figure 8c) is linear and overlies the one-to-one line but has a slight discontinuity near a chlorophyll value of 3. This indicates that some parameter modifications for the packaged algorithm are needed in this transition region.

Using the blended algorithm on 326 data points, the r^2 increased to 0.951 while the other statistics remained about the same (Table 4). The RMS2 error of about 28% for the packaged algorithm also is better than our accuracy goal of 35% or less.

4.6. Algorithm Evaluation With a Global Data Set

To generate an algorithm to smoothly transition between regions and periods where there are packaged and unpackaged pigments, we developed a global data set combining the packaged, unpackaged, and other mixed data sets from the SeaBASS archive. This data set has 976 data points. We then developed a set of compromise parameters for this global-average algorithm, shown in Table 3, for use at times and places where packaging is unknown or transitional. For this data set and these average parameters, 883 (90.5%) of the points passed the semianalytical portion of the algorithm, yielding RMS1 and RMS2 errors in algorithm-derived [chl *a*] of 0.176 and 0.446, respectively. The type II RMA slope was 1.003, the bias was 0.002, and r^2 was 0.852. Statistics for the entire n=976 set were similar, except r^2 was higher (0.913) (Table 4). The scatterplot (Figure 9a) looks evenly clustered about the one-to-one line, and the quantile plot (Figure 9c), though sinuous, overlays the one-to-one line for the most part. Again, the results from the semianalytical algorithm fall below those for the default algorithm near the transition region. This can be alleviated by reducing the "blending" domain from $0.015 < a_\phi(675) < 0.03$ to $0.008 < a_\phi(675) < 0.015$.

If we are unable to accurately specify the packaging domains of the world ocean, such a compromise global algorithm with about 44% accuracy is likely to be the best accuracy that can be achieved. This does not meet our accuracy goal of 35% or better, so a focused effort is being made to develop an accurate sorting mechanism based on space-derived data to define the bio-optical domains of the ocean on a spatial and temporal basis.

5. Discussion

The biggest limitation to algorithm development for the global ocean is a paucity of bio-optical field data from around the globe that are complete with ancillary particle and gelbstoff absorption spectra and auxiliary data such as sea-surface temperature, salinity, and nutrients. These data are needed in order to assess the spatial and temporal variation in the key algorithm parameters: X, Y, S, and, most important, $a_0(\lambda)$ and $a_1(\lambda)$. In order to derive [chl *a*], it is vitally important to be able to predict how the $a_\phi(\lambda)$/[chl *a*] ratio varies. Thus we must study the effect of light history, which is related to season, cloudiness, and latitude, as well as nutrient history, which is influenced by mixed-layer depth, upwelling, river plumes, and offshore/onshore proximity.

While algorithms appropriate for regions with strictly packaged or unpackaged pigments can reduce the uncertainty in chlorophyll *a* concentration from perhaps 45-50% to less than 30%, methods based upon space-derived data that determine when and where to apply the appropriate parameterization are still under development. One method using space-derived data numerical filter 2 has already been discussed, but it is only definitive for waters where $r_{25} > 3.0$. Also, stations with high gelbstoff concentrations can cause confusion using this method, and inaccurate atmospheric correction

can cause confusion using this method on any given day. For offshore oligotrophic to mesotrophic waters, however, it is a very useful diagnostic tool if used under clear atmospheric conditions.

A second space-based approach uses the fact that unpackaged pigments are usually found in high-light, nutrient-poor waters where small-diameter phytoplankton cells predominate [e.g., *Herbland et al.*, 1985; *Carder et al.*, 1986]. Since dissolved nutrients cannot be detected from space, a nutrient surrogate was sought. *Kamykowski* [1987] developed a model that explained much of the covariance observed between upper layer temperatures and nitrate concentrations [e.g., *Kamykowski and Zentara*, 1986]. D. Kamykowski (personal communication, 1998) has since developed nitrate-depletion temperatures (NDTs) for the North Atlantic Ocean. The nitrate-depletion temperature is defined as that temperature at which nitrate could no longer be detected, at least using techniques of the era from about 1960-1985. These NDTs provide a means to observe from space a variable that indicates when and where nitrate may be limiting phytoplankton growth and where upper layer production is dependent upon recycled nitrogen. Such phytoplankton are typically small [*Herbland et al.*, 1985] with unpackaged pigments [*Carder et al.*, 1986].

To delimit regions of the North Atlantic Ocean that likely contain unpackaged pigments, we have compared sea-surface temperatures to Kamykowski's NDTs. Figure 10 shows annual trends in sea-surface temperature, CZCS pigment, and NDTs for the Gulf of Maine, Bermuda, and Barbados. The temperatures and pigments are 4-year (1982-85) monthly averages from the Advanced Very High Resolution Radiometer (AVHRR) and CZCS sensors archived by the Jet Propulsion Laboratory, Physical Oceanography, satellite data archive (USA_NASA_JPL_PODAAC_A005). Note that based on this

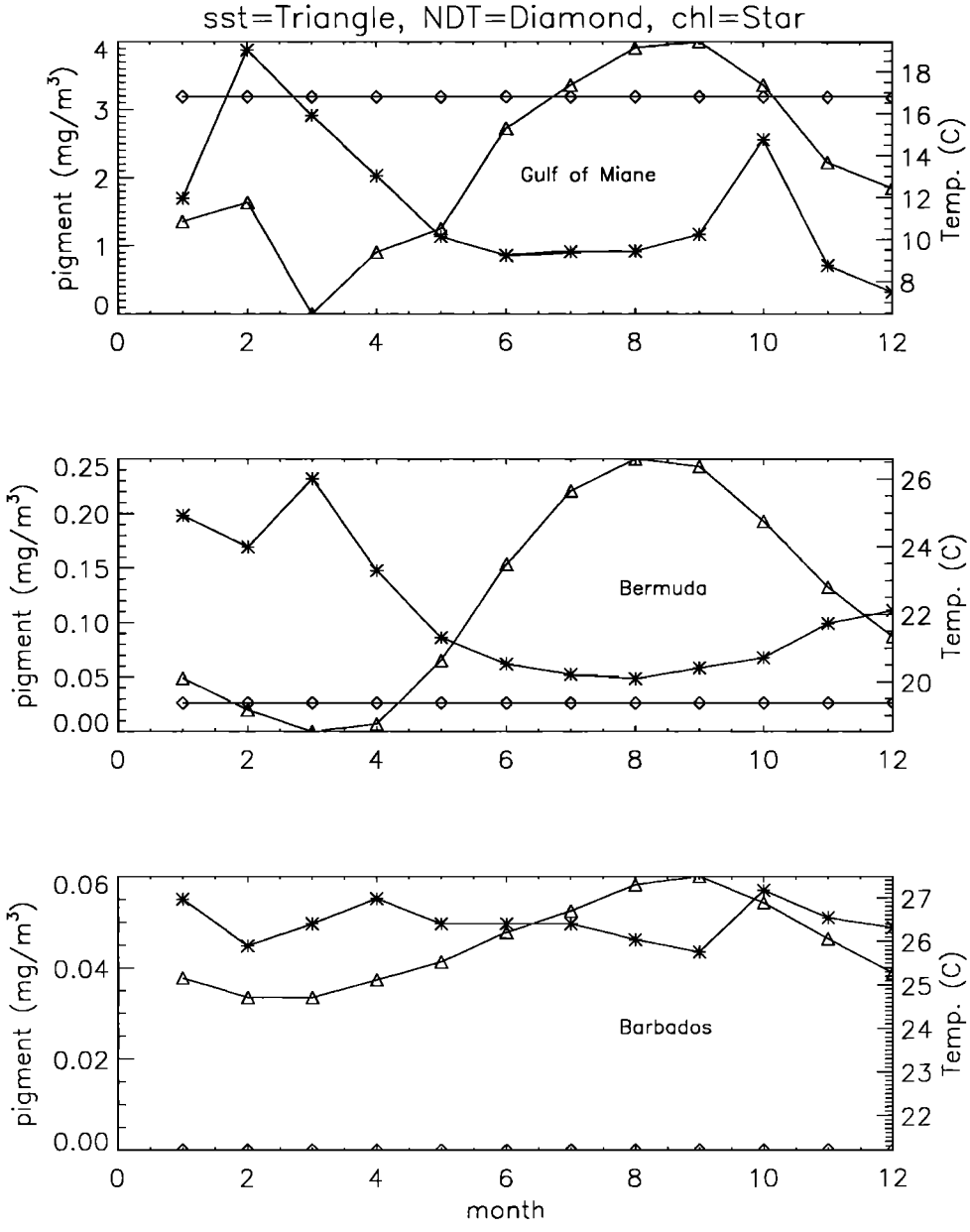

Figure 10. Four-year (1982-1985), monthly mean values of sea-surface temperature (triangles), CZCS pigment (asterisks), and nitrate-depletion temperature (diamonds) for locations near (top) the Gulf of Maine, (middle) Bermuda, and (bottom) Barbados.

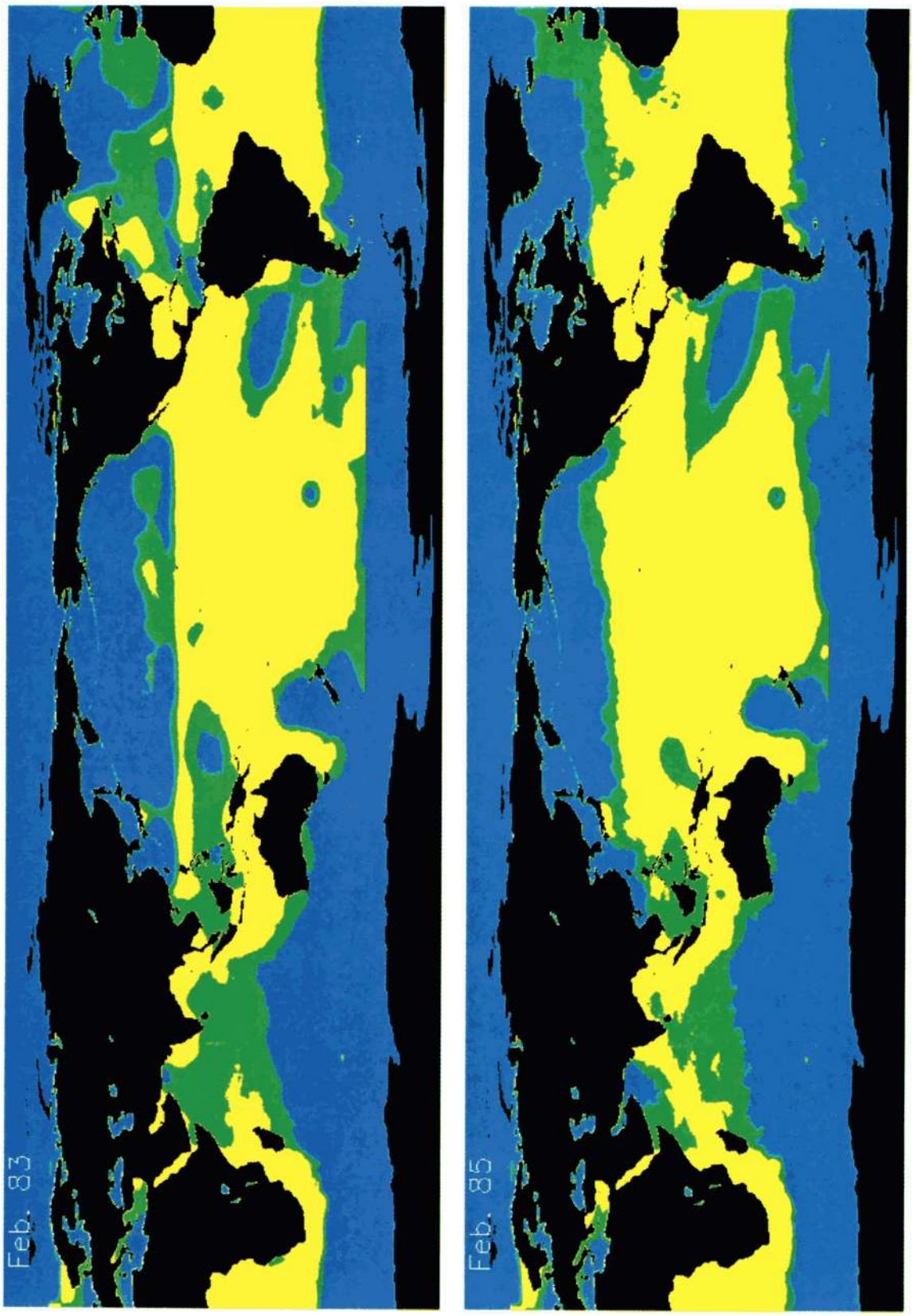

Plate 1. Bio-optical domains for the global ocean based on 1983 and 1985 monthly mean temperature compared to nitrate-depletion temperatures (NDTs) for (a) February and (b) August. Here black, blue, green, and yellow regions depict land, packaged, transitional, and unpackaged domains, respectively.

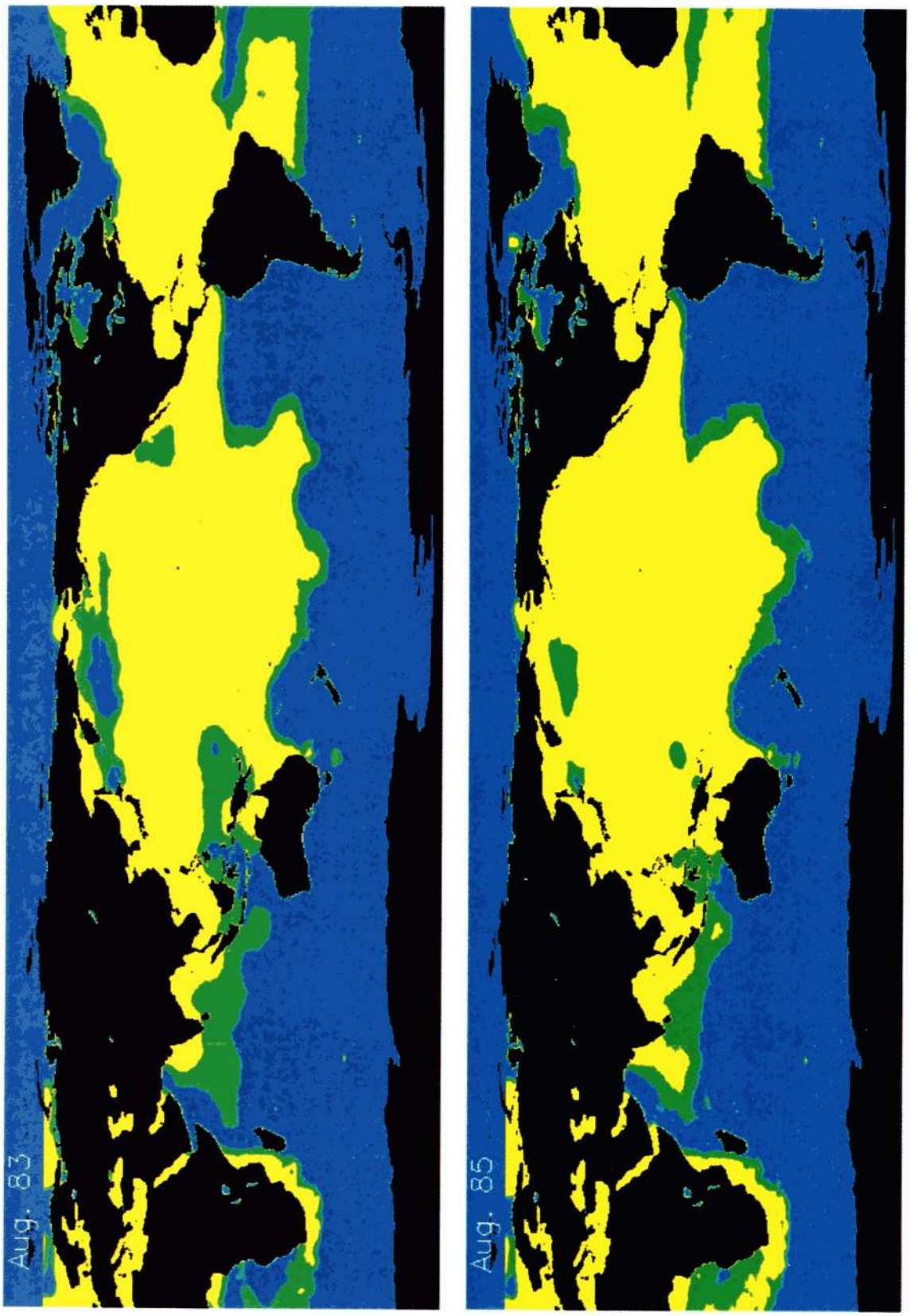

Plate 1. (continued)

approach, waters in the Gulf of Maine are rarely designated as being nitrogen limited, and those near Barbados are always designated as being nitrogen limited, while those near Bermuda are designated as being limited in the summer and unlimited in the winter-spring. Clearly, the Gulf of Maine is a lower-light, higher-nutrient environment than are Bermuda and Barbados, so the degree of packaging there is likely to be much higher.

By analyzing bio-optical data in the SeaBASS archive, some preliminary functional relationships between the NDTs and pigment-packaging classifications for the north Atlantic Ocean were empirically derived using sea-surface temperature (SST) derived from the AVHRR satellite sensor: (1) unpackaged domain: SST > NDT + 3.0° C, (2) transitional or global domain: NDT +1.8° C < SST < NDT + 3.0° C, and (3) packaged domain: SST < NDT + 1.8° C.

These domains for the months of February and August are shown for an El Niño year (1983) and a normal year (1985) in Plate 1, based upon climatological sea-surface temperatures. Here the tropics and most of the subtropics apparently contain phytoplankton with unpackaged pigments, except in the northwest African, Peruvian, and equatorial upwelling regions. Here transitional and packaged pigments can be observed during part of the year. High-latitude regions are mapped with this method as packaged and perhaps even hyperpackaged domains, gradually transitioning toward the equator into the unpackaged domain again. Note the marked difference in the domains between El Niño and "normal" years, especially in the tropics and subtropics.

Using AVHRR SST data from the physical oceanographic data archive, bio-optical data from SeaBASS for a cruise crossing several domains were sorted by domain using NDTs. Data for the transition period from spring to summer from the NASA SeaBASS archive were sorted into the three bio-optical domains, and the appropriate algorithm parameterization was applied to derive chlorophyll *a* values. May Atlantic Meridional Transect (AMT 4) data along 20° W longitude, North Sea data and MLML2 data collected in July, and GOMEX1 and GOMEX2 data collected in April and June provide a diverse set of north Atlantic observations that were sorted by the NDT filter and processed. The results (Figure 11) are compared with those obtained by simple use of the global (transitional) algorithm. The RMS1 and RMS2 errors for this diverse data set were 0.153 and 38%, respectively, for domain-sorted data, while the errors grew to 0.186 and 50%, respectively, when all were processed using global or transitional parameters for the algorithm without sorting by domain.

Since the spring-summer transition and eastern basin, upwelling data are perhaps the least predictable in terms of pigment packaging, the error reduction observed of 12% is indicative of the improvements that can be made by sorting ocean color data into bio-optical domains before applying algorithms. A community-wide effort to evaluate and modify this approach for other regions is an on-going task.

6. Conclusions

A MODIS semianalytical algorithm for chlorophyll *a* was tested using a total of 976 global data points from regions where the pigments were typically unpackaged, packaged,or transitional with appropriate algorithm parameters applied for each data type. The "unpackaged" type consisted of data sets that were generally consistent with the case 1 CZCS algorithm and consisted mostly of tropical, subtropical, and summer temperate data. This algorithm type was parameterized using Gulf of Mexico and Arabian Sea data. The "packaged" type consisted of eastern boundary upwelling data sets containing somewhat more packaged pigments. The packaged data sets were processed with the algorithm modified for phytoplankton-absorption parameters that were consistent with those of the South California Bight study area. This resulted in two fairly equally divided data sets totaling 604 points. That left 372 data points that were not well enough characterized to classify.

The semianalytical (SA) algorithm for chlorophyll *a* performed well on each of the data sets after classification, resulting in RMS1 errors of 0.099 and 0.111 (e.g., 0.10 log unit) for the unpackaged and packaged data classes, respectively, with little bias and with slopes near 1.0. RMS2 errors for the algorithms were 23% and 27%, respectively. The SA algorithm for phytoplankton absorption provided data accurate to about 30%.

While these numbers are excellent, one must bear in mind what misclassification does to the chlorophyll results. Using parameters for an average or transitional domain in the semianalytical MODIS algorithm with the global data set (n=976) yielded an RMS2 error of 44.6%, while applying the unpackaged parameters on the global evaluation data set yielded an RMS2 error of 92%. So, without classification, the algorithm performs better globally using the average parameters than it does if misclassification occurs.

For the difficult transition period between spring and summer, a data set was tested that included the eastern boundary region of the North Atlantic. Nitrogen-depletion temperatures were used with AVHRR-derived sea-surface temperatures to sort stations into

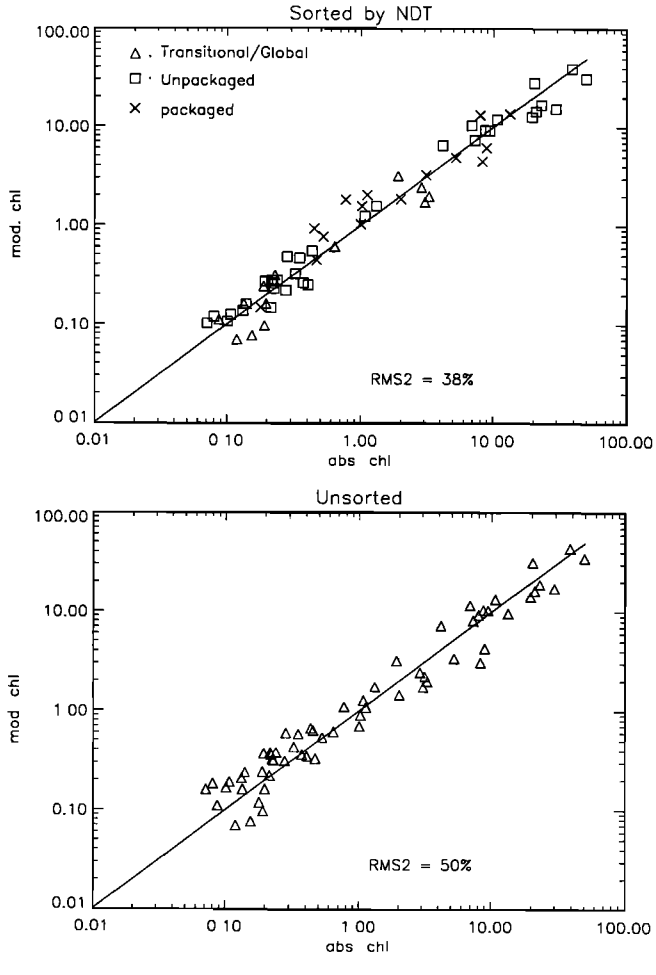

Figure 11. Comparisons of algorithm-derived and measured chlorophyll *a* values for (top) domain-sorted data for the North Atlantic Ocean during the spring-summer transitional period and (bottom) unsorted data.

packaged, unpackaged, and transitional domains. RMS2 errors dropped from 50% to 38% as a result of this data-sorting exercise. Since large regions of the subtropical and tropical Atlantic, Pacific, and Indian Oceans remain in the unpackaged bio-optical domain during all seasons and provide stable data accuracies from 24% to 28%, it is reasonable to expect that use of an NDT-based sorting algorithm with MODIS sea-surface temperatures to separate data into appropriate bio-optical domains will result in accuracies for the MODIS semianalytical chlorophyll *a* algorithm that are significantly lower than our target value of 35%.

Acknowledgments. Financial support was provided by NASA contract NAS5-31716 and NAGW465 and by ONR grant N00014-96-1-5013.

References

Aiken, J., G.F. Moore, C.C. Trees, S.B. Hooker, and D.K. Clark, The SeaWiFS CZCS-type pigment algorithm, in *SeaWiFS Technical Report Series*, vol. 29, edited by S.B. Hooker and E.R. Firestone, Goddard Space Flight Center, Greenbelt, MD, 1995.

Austin, R.W., Inherent spectral radiance signatures of the ocean surface, in *Ocean Color Analysis*, pp. 2.1-2.20, Scripps Institute of Oceanography, San Diego, CA, 1974.

Barnes, R.A., W.L. Barnes, W.E. Esaias, and C.R. McClain, Prelaunch acceptance report for the SeaWiFS radiometer, in *SeaWiFS Technical Report Series*, vol. 22, edited by S.B. Hooker, E.R. Firestone, and J. G. Acker, Goddard Space Flight Center, Greenbelt, MD, 1994.

Bissett, W.P., J.S. Patch, K.L. Carder, and Z.P. Lee, Pigment packaging and chlorophyll *a* specific absorption in high-light oceanic waters, *Proc. SPIE Int. Soc. Opt. Eng., 2963*, 358-374, 1997.

Bricaud, A., A. Morel, and L. Prieur, Absorption by dissolved organic matter in the sea (yellow substance) in the UV and visible domains, *Limnol. Oceanogr., 26*, 43–53, 1981.

Bricaud, A., et al., Variability in the chlorophyll-specific absorption coefficients of natural phytoplankton: Analysis and parameterization, *J. Geophys. Res., 100*: 13,321-13,332, 1995.

Carder, K.L., R.G. Steward, J.H. Paul, and G.A. Vargo, Relationships between chlorophyll and ocean color constituents as they affect remote sensing reflectance, *Limnol. Oceanogr., 31*, 403-413, 1986.

Carder, K.L., R.G. Steward, G.R. Harvey, and P.B. Ortner, Marine humic and fulvic acids: Their effects on remote sensing of ocean chlorophyll, *Limnol. Oceanogr., 34*, 68–81, 1989.

Carder, K.L., S.K. Hawes, K.A. Baker, R.C. Smith, R.G. Steward, and B.G. Mitchell, Reflectance model for quantifying chlorophyll *a* in the presence of productivity degradation products, *J. Geophys. Res., 96*, 20,599–20,611, 1991.

Gordon, H.R., and A. Morel, *Remote Assessment of Ocean Color for Interpretation of Satellite Visible Imagery: A Review*, Springer-Verlag, New York, 1983.

Gordon, H.R., and M. Wang, Retrieval of water-leaving radiance and aerosol optical thickness over the ocean with SeaWiFS: A preliminary algorithm, *Appl. Opt., 33*, 443-452, 1994.

Gordon, H.R., O.B. Brown, and M.M. Jacobs, Computed relationships between the inherent and apparent optical properties of a flat homogeneous ocean, *Appl. Opt., 14*, 417–427, 1975.

Gordon, H.R., D.K. Clark, J.W. Brown, O.B. Brown, R.H. Evans, and W.W. Broenkow, Phytoplankton pigment concentrations in the Middle Atlantic Bight: Comparison of ship determinations and CZCS estimates, *Appl. Opt., 22*, 20–36, 1983.

Gordon, H.R., O.B. Brown, R.H. Evans, J.W. Brown, R.C. Smith, K.S. Baker, and D.K. Clark, A semi-analytic model of ocean color, *J. Geophys. Res., 93*, 10,909–10,924, 1988.

Herbland, A., A. LeBouteiller, and R.Raimbault, Size structure of phytoplankton biomass in the equatorial Atlantic Ocean. *Deep Sea Res., Part A, 32*, 819-836, 1985.

Holm-Hanson, O., and E. Rieman, Chlorophyll-a determinations: improvement in methodology, *Oikos*, 30, 438-447, 1978.

Jerome, J.H., R.P. Bukata, and J.E. Burton, Utilizing the components of vector irradiance to estimate the scalar irradiance in natural waters, *Appl. Opt., 27*, 4012–4018, 1988.

Kamykowski, D., A preliminary biophysical model of the relationship between temperature and plant nutrients in the upper ocean, *Deep Sea Res., Part A, 34*, 1067–1079, 1987.

Kamykowski, D., and S.J. Zentara, Predicting plant nutrient concentrations from temperature and sigma-*t* in the upper kilometer of the world ocean, *Deep Sea Res., Part A, 33*, 89–105, 1986.

Kirk, J.T.O., *Light and Photosynthesis in Aquatic Ecosystems*, 401 pp., Cambridge Univ. Press, New York, 1983.

Kirk, J.T.O., Dependence of relationship between inherent and apparent optical properties of water on solar altitude, *Limnol. Oceanogr., 29*, 350–356, 1984.

Kirk, J.T.O., Volume scattering function, average cosines, and the underwater light field, *Limnol. Oceanogr., 36*, 455–467, 1991.

Lee, Z.P., K.L. Carder, S.H. Hawes, R.G. Steward, T.G. Peacock, and C.O. Davis, A model for interpretation of hyperspectral remote-sensing reflectance, *Appl. Opt., 33*, 5721–5732, 1994.

Lee, Z.P., K.L. Carder, R.G. Steward, T.G. Peacock, C.O. Davis, and J.L. Mueller, Remote-sensing reflectance and inherent optical properties of oceanic waters derived from above-water measurements, *Proc. SPIE Int. Soc. Opt. Eng., 2963*, 160–166, 1996.

Lee, Z.P., K.L. Carder, R.G. Steward, T.G. Peacock, C.O. Davis, and J.S. Patch, An empirical ocean color Algorithm for light absorption coefficients of optically deep waters, *J. Geophys. Res., 103*, 27,967-27,978, 1998.

Mitchell, B.G., Algorithms for determining the absorption coefficients for aquatic particulates using the Quantitative Filter Technique, in *Ocean Optics X, Proc. SPIE, Int. Soc. Opt. Eng., 1302*, 137–148, 1990.

Mitchell, B.G., and O. Holm-Hansen, Bio-optical properties of Antarctic waters: differentiation from temperate ocean models, *Deep Sea Res., Part A, 38*, 1009–1028, 1991.

Mobley, C.D., Light and Water, *592 pp.*, Academic, San Diego, Calif., 1994.

Moore, L.R., R. Goericke, and S.W. Chisolm, Comparative physiology of *Synechococcus* and *Prochlorococcus*: influence of light and temperature on growth, pigments, fluorescence and absorptive properties, *Mar. Ecol. Prog. Ser., 116*, 259–275, 1995.

Morel, A., and Y. Ahn, Optical efficiency factors of free-living marine bacterioplankton upon the optical properties and particulate organic carbon in oceanic waters, *J. Mar. Res., 48*, 145-147, 1990.

Morel, A., and Y. Ahn, Optics of heterotrophic nanoflagellates and ciliates: a tentative assessment of their scattering role in oceanic waters compared to those of bacterial and algal cells, *J.Mar.Res., 49*, 177-202, 1991.

Morel, A., and A. Bricaud, Theoretical results concerning light absorption in a discrete medium and application to the specific absorption of phytoplankton, *Deep Sea Res., Part A, 28*, 1357–1393, 1981.

Morel, A., and B. Gentili, Diffuse reflectance of oceanic waters: Its dependence on Sun angle as influenced by the molecular scattering contribution, *Appl. Opt., 30*, 4427–4438, 1991.

Morel, A., and B. Gentili, Diffuse reflectance of oceanic waters, II, Bi-directional aspects, *Appl. Opt., 32*, 6864–6879, 1993.

Morel, A., and B. Gentili, Diffuse reflectance of oceanic waters, III, Implication of bi-directionality for the remote sensing problem, *Appl. Opt., 35*, 4850–4862, 1996.

Morel, A., and H.R. Gordon, Report of the working group of water color, *Boundary Layer Meteorol., 18*, 343-355, 1980.

Morel, A., and L. Prieur, Analysis of variations in ocean color, *Limnol. Oceanogr., 22*, 709–722, 1977.

Morel, A., Y. Ahn, F. Partensky, D. Vaulot, and H. Claustre, *Prochlorococcus* and *Synechococcus*: A comparative study of their optical properties in relation to their size and pigmentation. *J. Mar. Res., 51*, 617-649, 1993.

Mueller, J.L., and R.W. Austin, Ocean optics protocols for SeaWiFS validation, revision 1, *NASA Tech. Memo. 104566*, vol. 25, 1995.

Nelson, J.R., and C.Y. Robertson, Detrital spectral absorption: Laboratory studies of visible light effects on phytodetritus absorption, bacterial spectral signal, and comparison to field measurements, *J. Mar. Res., 51*, 181–207, 1993.

O'Reilly, J.E., S. Maritorena, B.G. Mitchell, D.A. Siegel, K.L. Carder, S.A. Garver, M. Kahru, and C. McClain, Ocean color algorithms for SeaWiFS, *J. Geophys. Res., 103*, 24,937-24,953, 1998.

Peacock, T.G., K.L. Carder, P.G. Coble, Z.P. Lee, and S.K. Hawes,

Long-path spectrophotometer for measuring gelbstoff absorption in clear waters (abstract), *EOS, Trans., AGU, 75*, 22, 1994.

Peacock, T.P., K.L. Carder, and R.G. Steward, Components of spectral attenuation for an offshore jet in the Coastal Transition Zone, *Eos Trans. AGU, 69*, 1125, 1988.

Pope, R.M., and E.S. Fry, Absorption spectrum (380–700 nm) of pure water, II, Integrating cavity measurements, *Appl. Opt., 36*, 8710-8723, 1997.

Prieur, L., and S. Sathyendranath, An optical classification of coastal and oceanic waters based on the specific spectral absorption curves of phytoplankton pigments, dissolved organic matter, and other particulate materials, *Limnol. Oceanogr., 26*, 671-689, 1981.

Roesler, C.S., M.J. Perry, and K.L. Carder, Modeling *in situ* phytoplankton absorption from total absorption spectra in productive inland marine waters, *Limnol. Oceanogr., 34*, 1510–1523, 1989.

Sathyendranath, S., and T. Platt, Analytic model of ocean color, *Appl. Opt., 36*, 2620-2629, 1997.

Sathyendranath, S., T. Platt, C. Caverhill, R. Warnock, and M. Lewis, Remote sensing of oceanic primary production: Computations using a spectral model, *Deep Sea Res., Part A, 36*, 431-453, 1989.

Shibata, K., Spectrophotometry of intact biological materials. Absolute and relative measurements of their transmission, reflection and absorption spectra, *J. Biochem., 45*, 599–623, 1958.

Siegel, D., and A. Michaels, Quantification of non-algal light attenuation in the Sargasso Sea: Implications for biogeochemistry and remote sensing, *Deep Sea Res., Part II, 43*, 321-345, 1996.

Smith, R.C., and K.S. Baker, Optical properties of the clearest natural waters (200-800nm), *Appl. Opt., 20*, 177-184, 1981.

K. L. Carder, F. R. Chen, S. K. Hawes, and Z. P. Lee, Department of Marine Science, University of South Florida, 140 7th Avenue South, St. Petersburg, FL 33701. (e-mail: kcarder@monty.marine.usf.edu; chen@monty.marine.usf.edu; ska@monty.marine.usf.edu; zplee@monty.marine.usf.edu)

D. Kamykowski, Department of Marine, Earth, and Atmospheric Sciences, North Carolina State University, Box 8208, Raleigh, NC 27695. (e-mail: dan_kamykowski@ncs.edu)

(Received November 24, 1997; revised November 13, 1998; accepted November 18, 1998.)